Cell Metabolism

Article

Tumor aerobic glycolysis confers immune evasion through modulating sensitivity to T cell-mediated bystander killing via TNF-α

Graphical abstract

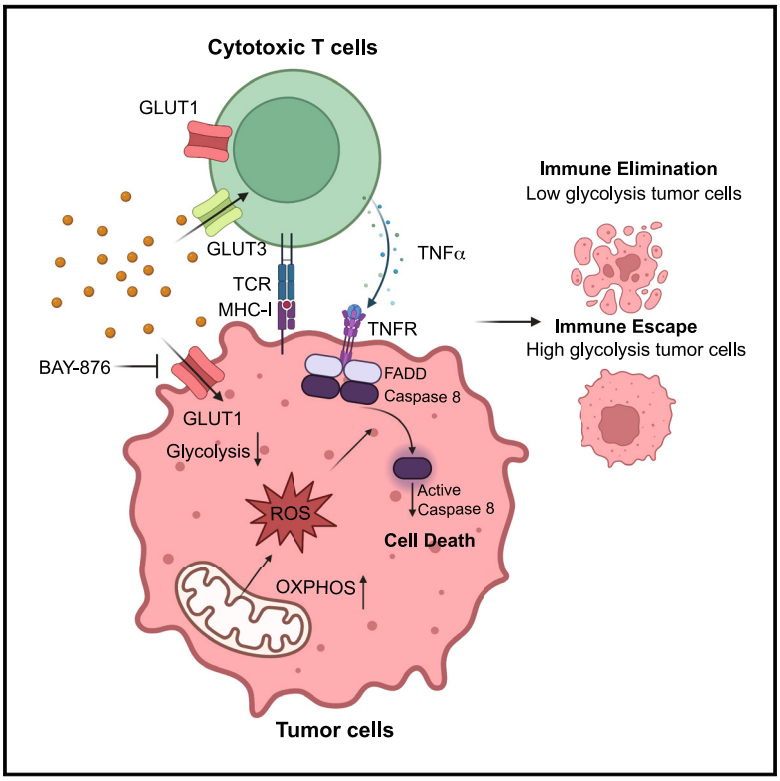

Highlights

- Tumor-intrinsic glycolysis pathway confers resistance to T cell-mediated killing
- Loss of Glut1 sensitizes tumor cells to TNF-α-induced cell death via elevated ROS
- Glut1 and Glut3 are differentially expressed in tumor and immune cells
- Inhibition of Glut1 potentiates anti-tumor immunity in mouse models

Authors

Lijian Wu, Yiteng Jin, Xi Zhao, ..., Fubing Wang, Zexian Zeng, Deng Pan

Correspondence

wangfubing@znhospital.cn (F.W.), zexianzeng@pku.edu.cn (Z.Z.), dpan@tsinghua.edu.cn (D.P.)

In brief

Wu et al. report that inhibition of the tumor-intrinsic glycolysis pathway by targeting Glut1 leads to accumulated intracellular ROS, which sensitized tumor cells to T cell-mediated bystander killing through TNF-α. Treatment with a Glut1-specific inhibitor sensitizes tumors to anti-tumor immunity and synergizes with anti-PD-1 therapy in mouse models.

Wu et al., 2023, Cell Metabolism *35*, 1–17
September 5, 2023
https://doi.org/10.1016/j.cmet.2023.07.001

CellPress

Cell Metabolism

CellPress

Article

Tumor aerobic glycolysis confers immune evasion through modulating sensitivity to T cell-mediated bystander killing via TNF-α

Lijian Wu,[1] Yiteng Jin,[2] Xi Zhao,[1] Kaiyang Tang,[1] Yaoning Zhao,[1] Linjie Tong,[1] Xuerong Yu,[1] Ke Xiong,[1] Ce Luo,[2] Jiajun Zhu,[1,4] Fubing Wang,[3,*] Zexian Zeng,[2,4,*] and Deng Pan[1,4,5,*]

[1]Department of Basic Medical Sciences, Tsinghua University, Beijing 100084, China
[2]Center for Quantitative Biology, Academy for Advanced Interdisciplinary Studies, Peking University, Beijing 100084, China
[3]Department of Laboratory Medicine, Zhongnan Hospital of Wuhan University, Wuhan 430071, China
[4]Tsinghua-Peking Center for Life Science (CLS), Beijing 100084, China
[5]Lead contact
*Correspondence: wangfubing@znhospital.cn (F.W.), zexianzeng@pku.edu.cn (Z.Z.), dpan@tsinghua.edu.cn (D.P.)
https://doi.org/10.1016/j.cmet.2023.07.001

SUMMARY

Metabolic reprogramming toward glycolysis is a hallmark of cancer malignancy. The molecular mechanisms by which the tumor glycolysis pathway promotes immune evasion remain to be elucidated. Here, by performing genome-wide CRISPR screens in murine tumor cells co-cultured with cytotoxic T cells (CTLs), we identified that deficiency of two important glycolysis enzymes, Glut1 (glucose transporter 1) and Gpi1 (glucose-6-phosphate isomerase 1), resulted in enhanced killing of tumor cells by CTLs. Mechanistically, Glut1 inactivation causes metabolic rewiring toward oxidative phosphorylation, which generates an excessive amount of reactive oxygen species (ROS). Accumulated ROS potentiate tumor cell death mediated by tumor necrosis factor alpha (TNF-α) in a caspase-8- and Fadd-dependent manner. Genetic and pharmacological inactivation of Glut1 sensitizes tumors to anti-tumor immunity and synergizes with anti-PD-1 therapy through the TNF-α pathway. The mechanistic interplay between tumor-intrinsic glycolysis and TNF-α-induced killing provides new therapeutic strategies to enhance anti-tumor immunity.

INTRODUCTION

Failure to respond to immunotherapy, such as immune checkpoint blockade (ICB), is a major problem in cancer therapy. The resistance mechanisms operate in part through tumor-intrinsic resistance to killing mediated by cytotoxic T cells (CTLs). CTLs are the key effector cells of the anti-tumor immune response based on their ability to specifically recognize tumor cells through the interaction of T cell receptors (TCRs) and peptide-major histocompatibility complexes (MHCs).[1] Upon recognition, CTLs release cytotoxic granules that contain perforin and granzyme B. Perforin forms pores to facilitate the entry of granzyme B, which cleaves a number of substrates to induce apoptosis of target cells.[2] Consequently, tumors often develop a variety of resistance mechanisms to avoid recognition and killing mediated by CTLs. These mechanisms include downregulation of the antigen presentation pathway[3,4] and upregulation of immunosuppressive molecules such as PD-L1 and SERPINB9.[5,6] In addition to granzyme-dependent killing, T cells release cytokines such as TNF-α and IFNγ to change the tumor microenvironment (TME), including the behavior of tumor cells. In particular, TNF-α signaling is critical for the T cell-mediated killing of tumor cells. The engagement of TNF-α with TNF receptor (TNFR) triggers a set of opposing signals in the tumor cells, including survival signals mediated by NF-κB and cell death signals induced by the formation of apoptosis/necrosis complexes.[7] It has been shown that genetic deletion of key regulators of TNF-α-mediated survival signals, including *TRAF2*, *RNF31*, and *RIPK1*, sensitizes tumor cells to T cell-mediated killing and ICB treatment in multiple murine tumor models.[8–12] These findings underscore the important role of the TNF-α signaling pathway in resistance to CTL-mediated killing.

Metabolic adaptation toward aerobic glycolysis is a common feature of cancer cells.[13] It has been documented that the glycolysis pathway contributes to immune evasion through several mechanisms. First, the tumor and immune cells compete for nutrients in the TME. For example, tumors with a high glucose uptake rate compete for glucose with T cells, which also rely on glycolysis for their anti-tumor functions.[14,15] Second, byproducts of aerobic glycolysis, such as lactate, can suppress T cell proliferation by impairing the glycolysis activity of T cells.[16] Third, the tumor glycolysis pathway can directly modulate the expression of many immunomodulatory molecules, such as CXCL10 and PD-L1.[17,18] Although the glycolysis pathway is related to immune evasion, it remains unclear whether and how the tumor

Please cite this article in press as: Wu et al., Tumor aerobic glycolysis confers immune evasion through modulating sensitivity to T cell-mediated bystander killing via TNF-α, Cell Metabolism (2023), https://doi.org/10.1016/j.cmet.2023.07.001

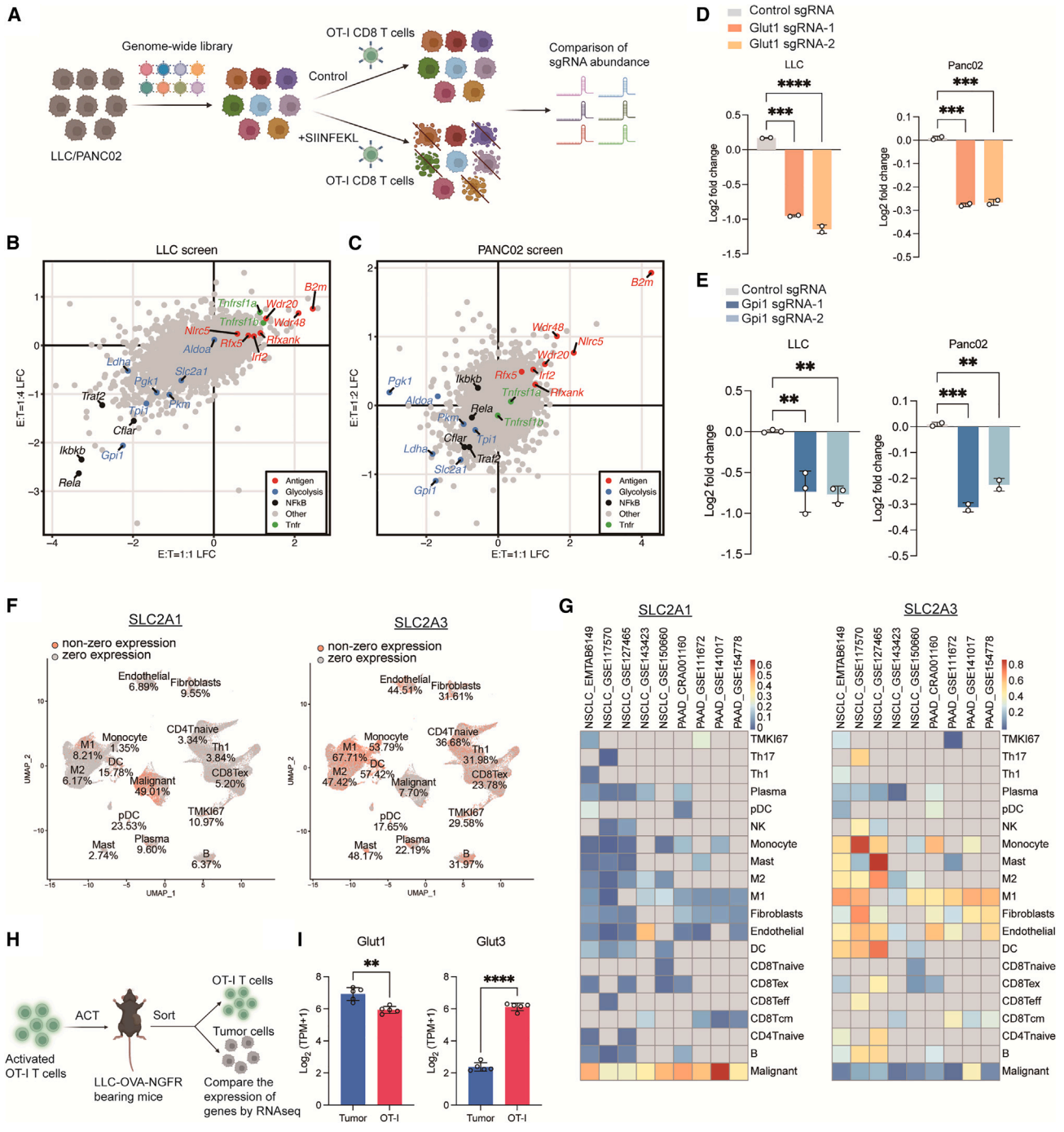

Figure 1. Genome-wide CRISPR screen reveals that inactivation of Glut1, a preferentially expressed glucose transporter in cancer cells, sensitized T cell-mediated killing of tumor cells

(A) Workflow of tumor-CTL co-culture screens.

(B and C) Scatterplot of top enriched and depleted sgRNAs based on mean $\log_2$ fold change of sgRNA counts in SIINFEKL pulsed compared with unpulsed condition in LLC (B) and Panc02 (C) screens using of two E:T ratios. Annotated genes represent MHC class I antigen presentation (red), TNF-α-induced NF-κB pathway (black), TNF-α receptors (green), and glycolysis pathway (blue).

(D and E) *In vitro* competition assay based on tumor-CTL co-culture. GFP-labeled LLC or Panc02 cells were mixed with either cells transduced with control sgRNA (sgControl), sgRNA targeting Glut1 (sgGlut1) (D, n = 2), or sgRNA targeting Gpi1 (sgGpi1) (E, n = 3 for LLC and n = 2 for Panc02). The cell mixtures were pulsed with SIINFEKL peptide and then co-cultured with pre-activated OT-I T cells. $\log_2$ fold change of the percentage KO cells upon co-culture with OT-I T cells was shown.

(F) UMAP plots of expression of SLC2A1 and SLC2A3 of cells in NSCLC_E-MTAB-6149 cohort, with expression frequency annotated under each cell type.

(G) Heatmaps of expression frequency of SLC2A1 and SLC2A3 of each cell type in multiple cancer cohorts.

(legend continued on next page)

Please cite this article in press as: Wu et al., Tumor aerobic glycolysis confers immune evasion through modulating sensitivity to T cell-mediated bystander killing via TNF-α, Cell Metabolism (2023), https://doi.org/10.1016/j.cmet.2023.07.001

glycolysis pathway directly confers resistance to the immune-mediated killing process.

In the current study, we performed genome-wide CRISPR-Cas9 screening in two murine cancer cell lines to identify the mechanisms of resistance to CTL-mediated killing. We found that inactivation of the tumor-intrinsic expression of two enzymes of the glycolysis pathway, Glut1 (glucose transporter 1) and Gpi1 (glucose-6-phosphate isomerase 1), sensitized tumor cells to CTL-mediated killing. Mechanistically, a compromised glycolysis pathway in tumor cells resulted in higher levels of reactive oxygen species (ROS), which could be generated by increased levels of mitochondrial respiration. Consequently, elevated cellular ROS potentiates CTL-mediated bystander killing through TNF-α induced cell death by downregulating c-FLIP, a key repressor of TNF-α-induced cell death. Importantly, Glut1 is highly expressed in tumors as compared with immune cells, whereas Glut3 is highly expressed in T cells, suggesting that Glut1 is a potential immunotherapy target. We further performed animal experiments and showed that Glut1 inhibition by small-molecule inhibitors sensitized tumor cells to ICB in a TNF-α-dependent manner. Thus, the interplay between tumor glycolysis and TNF-α-induced cell death provides new therapeutic opportunities to boost anti-tumor immunity.

RESULTS

Genome-wide CRISPR screens identified tumor-intrinsic glycolysis pathways that confer resistance to T cell-mediated killing

To better understand the tumor-intrinsic resistance mechanisms in CTL-mediated killing, we performed genome-wide CRISPR screening in cancer cell lines to test their perturbation effects when co-cultured with CTLs. The murine lung cancer cell line (LLC) and pancreatic cancer cell line (Panc02) were transduced with a genome-wide sgRNA library. Edited tumor cells were then pulsed with the SIINFEKL peptide and incubated with pre-activated OT-I CTLs to induce antigen-specific killing. Depletion of key targets would induce T cell killing and thus result in depletion of the corresponding gRNAs. For each screen, we used two effector-to-target ratios to induce strong or weak killing of tumor cells (Figure 1A). Representation of gRNAs was quantified by deep sequencing of the gRNA cassette with or without pulsing SIINFEKL peptide. In agreement with other similar tumor-T cell co-culture CRISPR screens, sgRNAs targeting positive regulator of MHC-I expression and antigen presentation (*B2m*, *Nlrc5*, *Rfxank*, and *Rfx5*) were enriched upon killing by CTLs (Figures 1B and 1C).[19,20] In addition, sgRNAs targeting genes associated with the TNF-α-induced NF-κB pathway were strongly depleted in both screens (*Traf2*, *Cflar*, *Ikbkb*, and *Rela*), and that targeting TNF-α receptors (*Tnfrsf1a* and *Tnfrsf1b*) were strongly enriched in LLC screens (Figures 1B and 1C). These results were in line with previous reports that depletion of TNF-α-induced NF-κB pathway induces tumor cell resistance to T cell killing.[8–11] Noticeably, sgRNAs targeting several key glycolysis enzymes were strongly depleted in both screens, including *Slc2a1* (Glut1), *Gpi1*, *Pkm* (pyruvate kinase 1), and *Ldha* (lacate dehydrogenase A) (Figures 1B and 1C). The depletion of sgRNAs targeting the glycolysis pathway, particularly Glut1 and Gpi1, was also consistently observed in several previous tumor-CTL co-culture screening experiments using different TCRs[8,19,20] (Figure S1A). These data indicate that targeting genes in the glycolysis pathway in tumor cells has a potential to enhance their vulnerability to T cell-mediated killing.

As glycolysis is a housekeeping pathway essential for cell survival,[21] we sought to identify glycolysis genes that are selectively required for conferring the resistance to T cell-mediated killing but are less essential for cell survival. By comparing the changes in sgRNA abundance under normal cell culture conditions, we found that loss of function of Glut1 and Gpi1 had a relatively mild effect on tumor growth compared with that of other glycolysis enzymes (e.g., *Pgk1*, *Pkm*, *Ldha*, and *Aldoa*) (Figures S1B and S1C). The low essentiality of GLUT1 and GPI (the human homolog of murine *Gpi1*) was further confirmed by analyzing 1,086 human cancer cell lines from the Depmap project (Figure S1D). We observed a strong correlation between the GLUT1 essentiality score (high score indicating lower essentiality) and the expression level of GLUT3 (Figure S1E), suggesting that the expression of GLUT3 might compensate for glucose transport upon Glut1 inactivation. In LLC cells, we confirmed that Glut3 is expressed, albeit at lower levels as compared with Glut1 (Figure S1F). We generated GLUT3 knockout (KO) LLC cells (KO efficiency = 82.2% based on TIDE analysis) to investigate whether GLUT3 expression could compensate for the loss of GLUT1. Under baseline conditions, we observed no effect on cell proliferation upon KO of GLUT3 (Figure S1G). However, when treated with the GLUT1 specific inhibitor BAY-876,[22] GLUT3-deficient cells showed increased sensitivity to the treatment, suggesting that GLUT3 plays a compensatory role upon GLUT1 inactivation (Figure S1G).

In contrast to their low essentiality in cell survival, KO of Glut1 and Gpi1 substantially sensitized LLC and Panc02 cells to CTL-mediated killing (Figures 1B and 1C). To validate this phenotype, we generated Glut1 and Gpi1 KO LLC and Panc02 cell lines by CRISPR-mediated mutagenesis (Figure S2A). Co-culture of KO tumor cells with T cells confirmed that inactivation of Glut1 or Gpi1 strongly sensitized tumor cells to T cell-mediated killing in LLC and Panc02 cells (Figures 1D, 1E, S2B, and S2C). Taken together, these data suggest that Glut1 and Gpi1 are selectively important for tumor cells to resist CTL-mediated cytotoxicity.

Differential expression patterns of glucose transporters in tumor and immune cells

The glycolysis pathway is essential for both tumor and immune cells.[23] To identify potential targets of glycolysis in cancer immunotherapy, we evaluated the expression patterns of glycolysis genes in published single-cell datasets. Among the examined glycolysis genes, we found that GLUT1 was highly expressed in most cancer cells, but relatively low in immune cells

(H) Workflow of OT-I adoptive transfer experiment.

(I) The expression level (log_2 (TPM + 1)) of Glut1 and Glut3 in sorted tumor and T cells, respectively (n = 5).

Data are represented as means ± SD (D, E, and I). *p < 0.05, **p < 0.01, ***p < 0.001, and ****p < 0.0001 by one-way ANOVA (D and E) and unpaired Student's t test (I). Data are representative of two independent experiments (D and E).

Please cite this article in press as: Wu et al., Tumor aerobic glycolysis confers immune evasion through modulating sensitivity to T cell-mediated bystander killing via TNF-α, Cell Metabolism (2023), https://doi.org/10.1016/j.cmet.2023.07.001

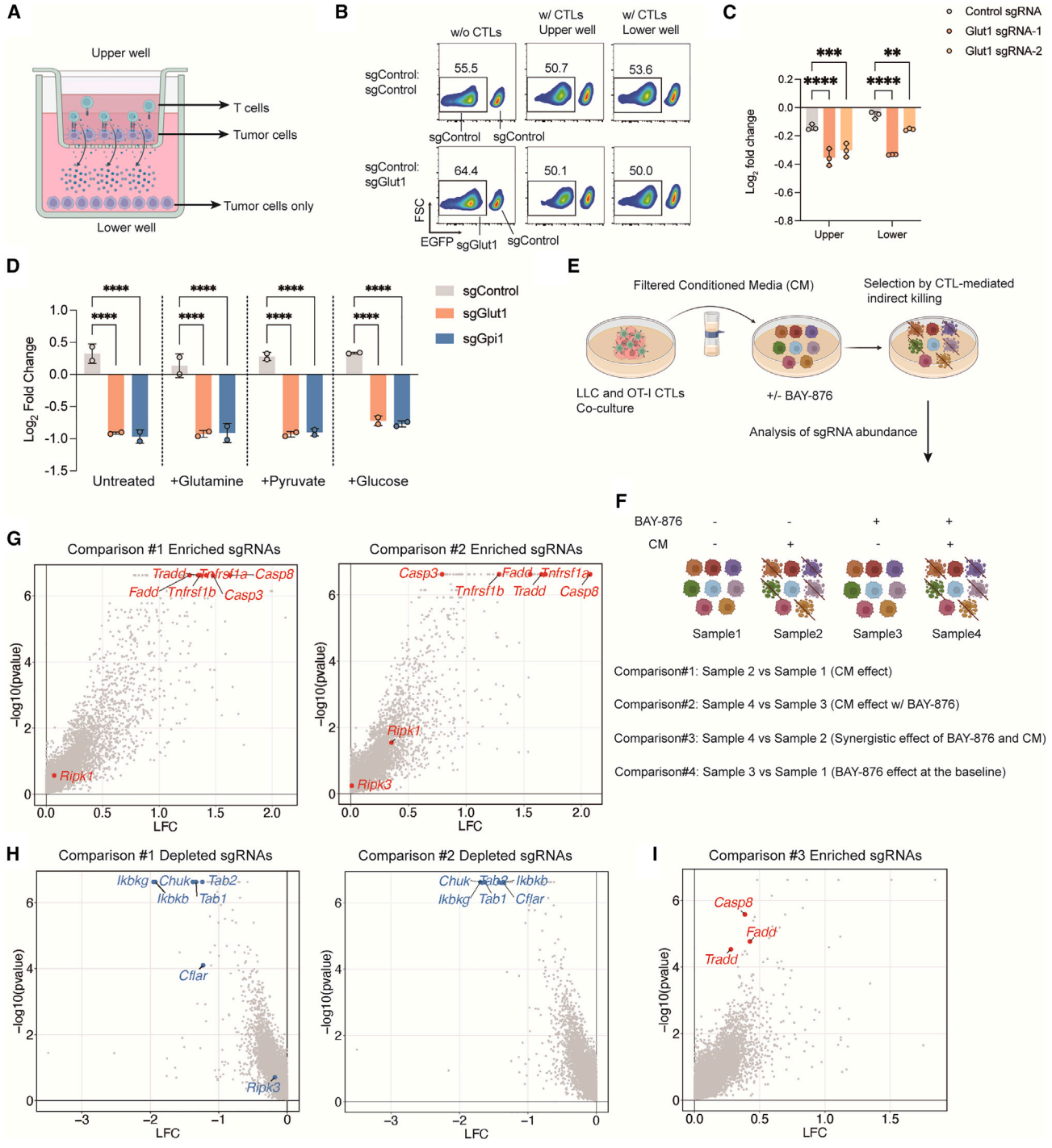

Figure 2. Glut1 inhibition sensitized tumors to T cell-mediated bystander killing via TNF-α pathway

(A) Illustration of tumor-T cell co-culture experiments performed in Transwell.

(B and C) In the Transwell experiment, representative FACS results (B) and summary of the $\log_2$ fold change (C, n = 3) of the ratio of Glut1 KO cells in the upper and lower wells upon adding of OT-I T cells.

(D) Summary of $\log_2$ fold changes of the percentage of Glut1 and Gpi1 KO cells upon adding CM derived from LLC-T cell co-culture, either in the presence or absence of indicated metabolites (n = 2).

(E) Illustration of genome-wide CRISPR screens to identify pathways required for bystander killing mediated by CTLs with and without Glut1 inhibition.

(F) Four sets of comparisons of sgRNA counts were performed by MaGECK analysis as indicated.

(G and H) Scatterplot of $\log_2$ fold change and p values of top enriched (G) and depleted (H) sgRNA counts in comparison #1 and #2, respectively. Genes in the TNF-α-induced apoptosis and NF-kB pathway were highlighted in red and blue, respectively.

(legend continued on next page)

Please cite this article in press as: Wu et al., Tumor aerobic glycolysis confers immune evasion through modulating sensitivity to T cell-mediated bystander killing via TNF-α, Cell Metabolism (2023), https://doi.org/10.1016/j.cmet.2023.07.001

(Figures 1F, 1G, S2D, and S2E). In contrast, GLUT3 (encoded by *SLC2A3*), a high-affinity glucose transporter,[24] was scarcely expressed in cancer cells but highly expressed in immune cells (Figures 1F, 1G, S2D, and S2E). To validate the observation from single-cell RNA sequencing (scRNA-seq) data, we assessed the expression level of GLUT1 in tumor and immune cells by performing immunofluorescence (IF) staining of GLUT1, CD45, and Ki67 in histological samples acquired from patients with non-small-cell lung cancer (NSCLC), pancreatic adenocarcinoma (PAAD), and colon adenocarcinoma (COAD). In all three cancer types, we found higher expression levels of GLUT1 in non-immune cells (CD45−) as compared with that in immune cells (CD45+) (Figures S2F and S2G). To further compare the expression of glucose transporters in tumor and tumor-reactive T cells, we performed RNA-seq on adoptively transferred OT-I T cells and LLC-OVA cells, respectively (Figure 1H). We found that Glut1 is expressed at a high level in both OT-I T cells and tumor cells, with higher expression in the tumor cells (Figure 1I). In contrast, Glut3 is predominantly expressed in T cells but at a low level in tumor cells (Figure 1I). Taken together, the preferential usage of GLUT1 in tumor cells as compared with T cells provides a strong rationale for further investigation of GLUT1 as a potential glycolysis target in cancer immunotherapy.

Glut1 inhibition sensitizes tumor cells to CTL killing via TNF-α-mediated cell death

CTL killing involves direct killing mediated by apoptosis induced by granzymes and indirect killing induced by cytokines such as interferons and TNF-α.[10,11,19,25,26] We therefore designed a Transwell experiment in which tumor antigen-specific T cells were co-cultured with tumor cells in the upper well, and only tumor cells were seeded in the lower well. This design ensured that direct killing could only occur in the upper well, and indirect killing could occur in both upper and lower wells (Figure 2A). Glut1 and Gpi1 KO cells were depleted as compared with control in the lower well upon the addition of corresponding antigen-specific T cells (OT-I or Pmel-1) in the upper well, suggesting that inactivation of Glut1 or Gpi1 sensitized tumor cells to indirect killing mediated by CTLs (Figures 2B, 2C, and S3A–S3C). Consistent with the model of indirect killing, Glut1 and Gpi1 KO cells were strongly depleted upon treatment with conditioned media (CM) derived from tumor-T cell co-culture assay (Figure 2D). Nutrient supplementation to the CM failed to rescue the phenotype, suggesting that the sensitive phenotype in Glut1/Gpi1 KO is not due to competition of nutrient between tumor and T cells (Figure 2D).

To systematically understand how Glut1 modulates the indirect killing process mediated by CTL-mediated bystander killing, we performed another set of genome-wide CRISPR screens to identify the key factors involved in this process. As illustrated in Figure 2E, LLC-Cas9 cells were transduced with a genome-wide sgRNA library and then treated with the CM from activated T cells. In addition, treatment was performed either in the presence or absence of Glut1 specific inhibitor BAY-876. Therefore, four sets of sgRNA abundance were generated and leveraged to explore key factors involved in the TNF-α-induced killing with or without Glut1 inhibition (Figure 2F). Overall, CM treatment resulted in significant enrichment of sgRNA targeting TNF-α-induced apoptosis pathway, including TNFR (*Tnfrsf1a* and *Tnfrsf1b*) and apoptosis complex (*Tradd*, *Fadd*, and *Casp8*) (Figure 2G). CM treatment resulted in depletion of sgRNAs targeting repressors of TNF-α-induced cell death, such as IKK complex (*Ikbkb*, *Chuk*, and *Ikbkg*) and c-FLIP (encoded by *Clfar*) (Figure 2H). Of note, sgRNAs targeting the key effectors required for TNF-α-induced apoptosis (*Casp8*, *Fadd*, and *Tradd*) were enriched upon the combination of CM and BAY-876 as compared with CM treatment alone (Figure 2I), indicating that Glut1 inhibition further sensitized LLC cells to TNF-α-induced apoptosis.

To validate this finding, we treated LLC cells with two major cytokines released from T cells, including TNF-α and IFNγ. Glut1 and Gpi1 KO cells were significantly depleted upon treatment with TNF-α, but not IFNγ (Figures 3A and S3D). In both LLC and Panc02 cells, co-treatment with BAY-876 and TNF-α induced substantial cell death as compared with treatment with TNF-α alone (Figures 3B and 3C). Combination treatment of BAY-876 and TNF-α also induced substantially higher levels of cell apoptosis (Figure 3D). Similarly, BAY-876 treatment sensitized MIA Paca-2, a human pancreatic cancer cell line, to TNF-α-induced apoptosis (Figure S3E). To further confirm that TNF-α is required to sensitize Glut1 and Gpi1 KO tumor cells to CTL-mediated killing, we generated Glut1 and Gpi1 KO cells in the TNF-α receptor-KO (Tnfrsf1a KO) LLC cells (Figure 3E). By performing co-culture experiments using two E:T ratios, Tnfrsf1a KO abolished the enhanced killing phenotype in Glut1 and Gpi1 KO cells (Figures 3F and S3F). In line with this obversion, addition of TNF-α blocking antibodies rescued the sensitive phenotype of Glut1 KO cells to T cell-mediated killing (Figure 3G). These data collectively suggest that Glut1 KO LLC tumors are more sensitive to T cell-mediated killing through TNF-α.

TNF-α-induced cell death is modulated by three signaling complexes.[7] To test which signaling complex plays an interactive role with Glut1 inhibition, we generated a panel of LLC KO cell lines that were defective in TNF-α-induced NF-κB (*Ripk1* KO), apoptosis (*Casp8* KO and *Fadd* KO), and necrosis (*Ripk3* KO). Interestingly, we found that BAY-876 treatment sensitized control LLC cells to TNF-α-induced cell death to an extent similar to that induced by Ripk1 KO (Figure 3H). In comparison, inactivation of Casp8 and Fadd, but not Ripk3, largely rescued cell death induced by TNF-α and BAY-876 treatment (Figure 3H). This observation prompted us to investigate whether Glut1 inhibition directly potentiated the activation of apoptosis signaling upon TNF-α treatment. We found that the combination of TNF-α and BAY-876 treatment substantially enhanced the level of cleaved caspase-8 as compared with treatment with TNF-α alone (Figure 3I). Consistently, cleaved caspase-8 level was much higher in Glut1 and Gpi1 KO cells upon TNF-α treatment (Figure S3G).

(I) Scatterplot of $\log_2$ fold change and p values of top enriched sgRNA counts in comparison #3. Key effector genes in TNF-α-induced apoptosis pathway were highlighted in red.

Data are represented as mean ± SD (C and D). **p < 0.01, ***p < 0.001, and ****p < 0.0001 by two-way ANOVA (C and D). Data are representative of two independent experiments (B–D).

Please cite this article in press as: Wu et al., Tumor aerobic glycolysis confers immune evasion through modulating sensitivity to T cell-mediated bystander killing via TNF-α, Cell Metabolism (2023), https://doi.org/10.1016/j.cmet.2023.07.001

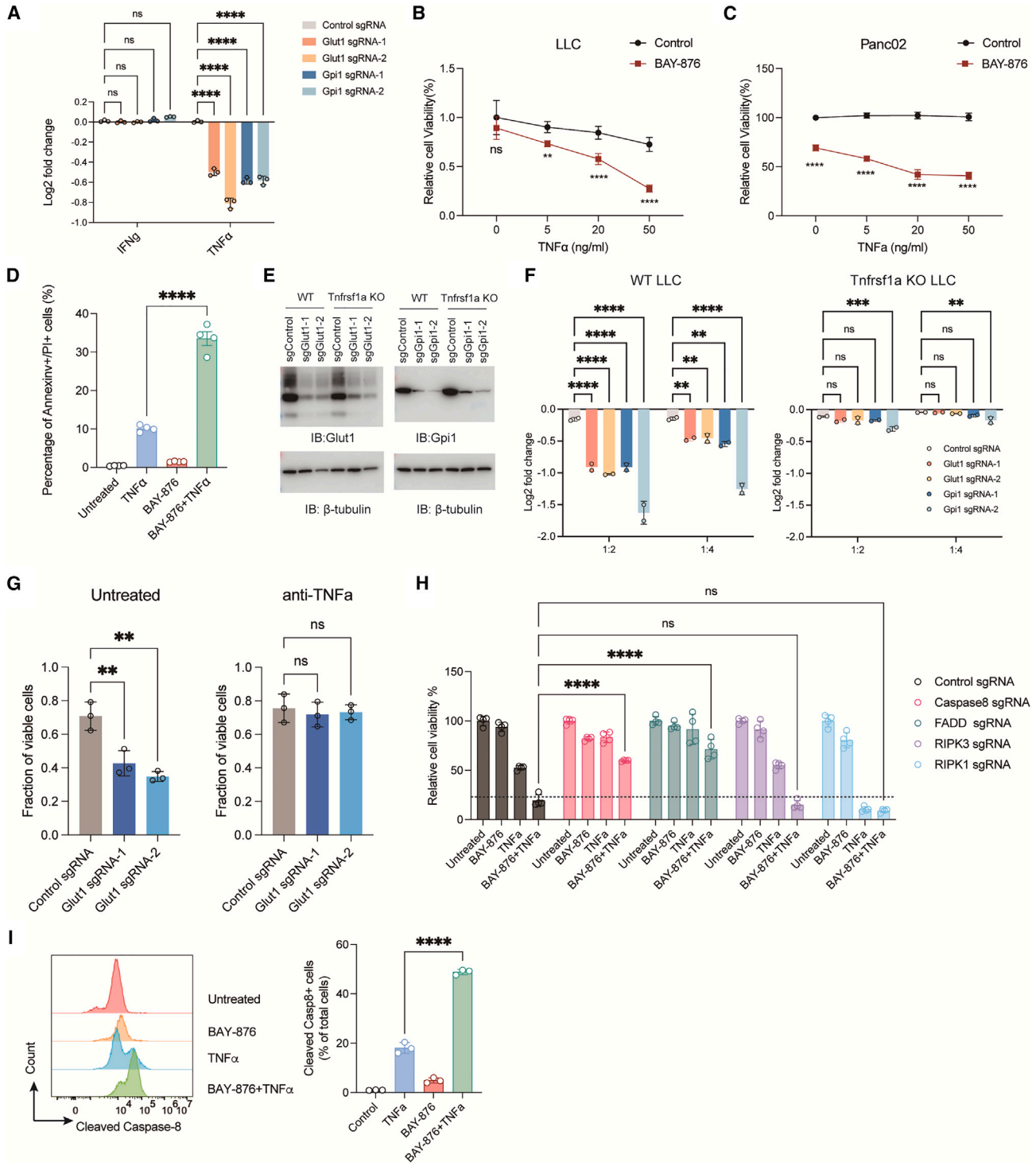

Figure 3. Inactivation of Glut1 sensitized tumor cells to TNF-α-mediated and caspase-8/Fadd-dependent cell death

(A) Summary of $\log_2$ fold changes of the ratio of Glut1 and Gpi1 KO cells upon treatment with indicated cytokines (50 ng/mL IFNγ or 50 ng/mL TNF-α for 48 h) (n = 3).

(B and C) LLC (B) and Panc02 (C) cells were treated with indicated doses of TNF-α in the presence or absence of BAY-876 (200 nM) for 24 h. The number of viable cells was determined by using CellTiter-Glo viability assay (n = 5).

(D) Annexin V and PI staining in LLC cells pretreated with BAY-876 (200 nM) for 24 h, followed by treatment with TNF-α (20 ng/mL) or left untreated for 48 h (n = 4).

(E) Glut1 and Gpi1 KO LLC cells were generated in wild-type and TNF receptor-KO (Tnfrsf1a KO) background, respectively. Western blot analysis of Glut1 and Gpi1 protein level in indicated cells.

(legend continued on next page)

Please cite this article in press as: Wu et al., Tumor aerobic glycolysis confers immune evasion through modulating sensitivity to T cell-mediated bystander killing via TNF-α, Cell Metabolism (2023), https://doi.org/10.1016/j.cmet.2023.07.001

Together, these data suggest that Glut1 inhibition potentiates TNF-α-induced activation of pro-apoptotic signaling.

Inhibition of glycolysis leads to higher cellular ROS, which potentiates TNF-α-induced apoptosis

To investigate the mechanisms underlying the potentiation of TNF-α-induced death by Glut1 inactivation, we profiled the transcriptome changes in LLC cells with treatment of TNF-α in the presence or absence of BAY-876. We analyzed the top 200 up- and downregulated genes by LISA, which uses a large collection of publicly available chromatin immunoprecipitation sequencing (ChIP-seq) results and known DNA-binding motifs to infer the altered transcriptional activities.[27] Both LISA and gene set enrichment analysis (GSEA) revealed a strong activation of ATF4 signaling upon BAY-876 treatment, either in the presence or absence of TNF-α (Figures 4A, 4B, and S4A). The activation of ATF4 was also confirmed at the protein level by western blot (Figure 4C). ATF4 is a major pathway activated by cellular stress from various sources, such as ROS.[28–32] Consistently, we found that BAY-876 treatment or Glut1 KO was sufficient to induce significantly higher levels of total and mitochondrial ROS (Figures 4D, S4B, and S4C).

Because oxidative phosphorylation (OXPHOS) is an important source of ROS production, we measured the rate of mitochondrial respiration and glycolysis following BAY-876 and TNF-α treatment in control and Glut1 KO cells, respectively. As expected, BAY-876 treatment and Glut1 KO resulted in a reduced level of aerobic glycolysis, as measured by the extracellular acidification rate (ECAR), proton efflux rate (PER), and glycolytic stress test (Figures 4E, 4F, and S4D–S4F). The treatment with BAY-876 or Glut1 KO resulted in a significantly higher level of OXPHOS in both the LLC and Pan02 cell lines (Figures 4E, 4F, and S4D), suggesting that Glut1 inhibition leads to a shift in the energy metabolism of the tumor cells toward OXPHOS. The effect of BAY-876 appeared to be specific to Glut1, as there was no additional effect on OCR/ECAR and ROS production when Glut1 KO cells were treated with BAY-876 (Figures S4C and S4D). Together, these data suggest that Glut1 inhibition caused a metabolic switch to mitochondrial respiration, which could contribute to the elevated cellular ROS.

Previous studies suggest that cellular ROS sensitizes cells to TNF-α-induced cell death through various mechanisms.[31–33] To determine whether the ROS generated upon Glut1 inhibition contributes to TNF-α-induced cell death, we treated LLC cells with 2-mercaptoethanol (2-ME), an antioxidant agent used to prevent toxic levels of oxygen radicals. 2-ME completely rescued mitochondrial ROS and the effect of synergistic cell death induced by BAY-876 and TNF-α (Figures 4G and 4H). 2-ME treatment also reduced the level of cleaved caspase-8 induced by TNF-α and BAY-876 (Figure 4I). It has been reported that the level of c-FLIP, a key repressor of TNF-α-induced apoptosis, is regulated by ROS.[34,35] We found that both RNA and protein level of c-FLIP were downregulated upon the combination treatment of TNF-α and BAY-876 as compared with TNF-α treatment alone (Figures S4G and S4H). Importantly, the downregulation of c-FLIP can be rescued by ROS scavenger NAC (N-acetyl-L-cysteine) (Figure S4H). Additionally, treatment of H_2O_2 substantially downregulated the protein level of c-FLIP (Figure S4I). These data suggest that ROS generated upon Glut1 inhibition contribute to the potentiation of TNF-α-induced cell death by downregulating c-FLIP.

Glut1 KO tumors were intrinsically sensitive to immune-mediated elimination through the TNF-α pathway

To understand whether and how the tumor-intrinsic glycolysis pathway affects tumor growth in the presence of immune selection pressure, we inoculated Glut1 KO and control LLC cells into immunodeficient NSG mice and immunocompetent wild-type B6 mice, respectively. Interestingly, Glut1 KO tumors grew at a rate comparable to that of the control in NSG mice (Figure 5A), suggesting that Glut1 is dispensable for tumor growth in the absence of immune selection pressure. In contrast, Glut1 KO tumors grew substantially slower than control tumors when they were engrafted into immune-competent mice (Figure 5B). A similar immune-dependent growth defect in Glut1 KO tumors was also observed in Panc02 tumors (Figures 5C and 5D). These results suggest that Glut1 is required for tumor growth when the host immune system is intact. Analysis of tumor-infiltrating lymphocytes (TILs) revealed substantially enhanced T cell infiltration in Glut1 KO tumors, including total CD45+ immune cells, CD8+ T cells, natural killer (NK) cells, and cytotoxic CD8+ T cells expressing granzyme B (GZMB+ CD8+) (Figures 5E–5H).

We next investigated whether Glut1 KO tumors were intrinsically more sensitive to anti-tumor immunity. To answer this question, we performed *in vivo* competition assays in which a mixture of Glut1 KO (tdTomato+) and control LLC cells (EGFP+) was engrafted in mice with different levels of immune selection pressure (Figure 5I). We found that Glut1 KO tumors were strongly depleted compared with control tumors in immune-competent mice as compared with tumors grew in immune-deficient mice (NSG) (Figures 5J and 5K). The depletion of Glut1 KO tumors was more substantial when mice were treated with anti-PD-1 (Figures 5J and 5K). Importantly, this depletion effect in Glut1 KO cells was abolished when Tnfrsf1a KO LLC cells were used (Figure 5L). Together, these data suggest that Glut1-deficient

(F) The summary of $\log_2$ fold change of the ratio of Glut1 and Gpi1 KO LLC cells, either in wild-type or TNF-α receptor-KO background, upon co-culture with OT-I T cells at indicated E:T ratios (n = 2).

(G) Control or Glut1 KO LLC cells were co-cultured with activated OT-I T cells in the presence or absence of anti-TNF-α-blocking antibodies. Relative number of viable tumor cells upon co-culture was shown (n = 3).

(H) Indicated control and KO LLC cells were treated with TNF-α (40 ng/mL), BAY-876 (200 nM), or combination of TNF-α and BAY-876 for 72 h. Cell viability was then measured by CellTiter-Glo assay (n = 4).

(I) The level of cleaved caspase-8 in LLC treated with TNF-α (20 ng/mL), BAY-876 (200 nM), or combination of TNF-α and BAY-876 for 48 h (n = 3). Representative flow cytometry plots (left) and summary of cleaved caspase-8-positive cells (right) were shown.

Data are represented as mean ± SD. $p < 0.05$, $^{**}p < 0.01$, $^{***}p < 0.001$, and $^{****}p < 0.0001$ by unpaired Student's t test (D and I), one-way ANOVA (G), and two-way ANOVA (A–C, F, and H). ns, not significant. Data are representative of at least 2 independent experiments (A–F, H, and I).

Please cite this article in press as: Wu et al., Tumor aerobic glycolysis confers immune evasion through modulating sensitivity to T cell-mediated bystander killing via TNF-α, Cell Metabolism (2023), https://doi.org/10.1016/j.cmet.2023.07.001

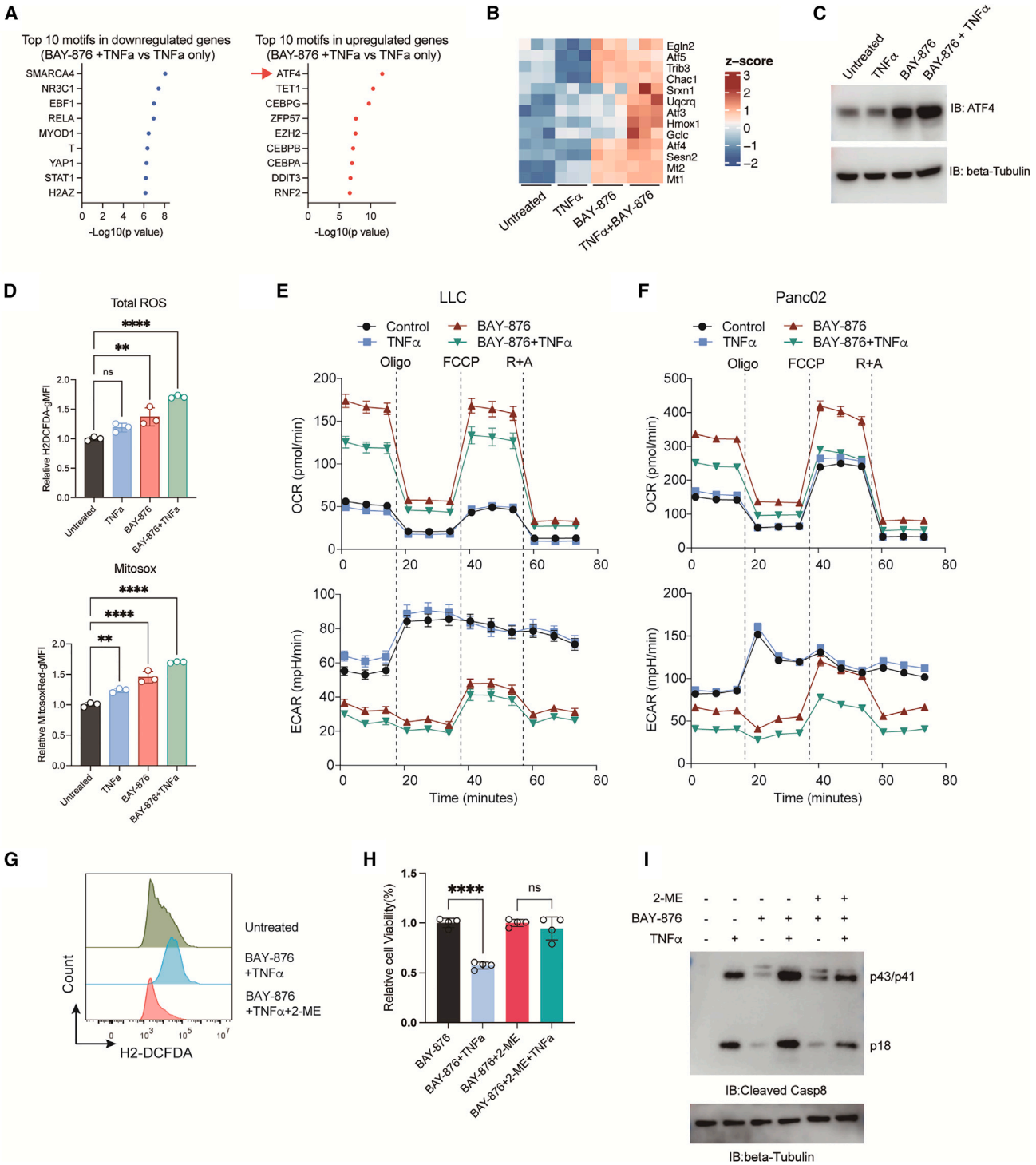

Figure 4. Glut1 inhibition potentiates TNF-α-induced cell death by ROS

(A) LISA analysis shows the top 10 enriched motifs for up- and downregulated genes comparing BAY-876 + TNF-α treatment versus TNF-α treatment alone in LLC cells.

(B) Heatmap showing the indicated ATF4 responsive genes under treatment of TNF-α (20 ng/mL), BAY-876 (200 nM), or in combination.

(C) Western blot analysis of ATF4 expression under the indicated conditions as in (B).

(D–F) Indicated cells were either pretreated with 200 nM BAY-876 or left untreated for 24 h, followed by treatment with 20 ng/mL TNF-α or left untreated for 24 h. H2-DCFDA (upper panel) and MitoSOX red staining (low panel) are shown in (D) (n = 3). Seahorse experiments were used to determine OCR and ECAR in LLC (E) and Panc02 cells (F) (n = 12).

(legend continued on next page)

cells are intrinsically sensitive to TNF-α-mediated immune selection *in vivo*.

Glut1 inhibitor BAY-876 potentiates anti-tumor immunity *in vivo* with enhanced levels of immune infiltration

To evaluate Glut1 as a potential drug target to boost anti-tumor immunity, we treated LLC tumors with Glut1-specific inhibitor BAY-876 or vehicle control through intratumor (i.t.) administration. Consistent with our data using genetic deletion of Glut1, BAY-876 treatment did not affect LLC tumor growth when tumors were engrafted into NSG mice (Figure 6A). In comparison, treatment with BAY-876 resulted in a substantial reduction in LLC tumor size in immune-competent mice and mice treated with anti-PD-1 (Figures 6B and 6C). BAY-876 inhibition also resulted in similar immune-dependent inhibition of tumor growth in the B16F10 and Panc02 tumor model (Figures S5A and S5B). We treated LLC tumors by intraperitoneal (i.p.) administration of BAY-876, and similar results were obtained (Figure S5C). Next, to determine whether the therapeutic effect of Glut1 inhibition was related to enhanced sensitivity to TNF-α, we repeated the experiments using Tnfrsf1a KO LLC cells. The deletion of TNFRs largely abolished the therapeutic effect of BAY-876, with or without combination with anti-PD-1 (Figures 6D and 6E). This suggests that the therapeutic effect of Glut1 inhibition operates through tumor-intrinsic TNF-α signaling.

To examine the effect of BAY-876 on the tumor immune microenvironment, we analyzed the number of TILs in the presence and absence of BAY-876 treatment in the LLC model. The combination of PD-1 and BAY-876 treatment resulted in a substantial increase in the number of infiltrating immune cells, including total CD45+ immune cells, CD4+ and CD8+ T cells, and NK cells (Figures 6F–6I). To better understand the impact of BAY-876 on other immune cells in the TME, we performed scRNA-seq on CD45+ immune cells isolated from LLC tumors treated with anti-PD-1 alone or in combination with BAY-876. Overall, the frequency of each major lineage in CD45+ immune cells was similar in BAY-876-treated tumors and controls (Figures 6J, 6K, S6A, and S6B). To investigate the potential impact of BAY-876 on T cells, we treated isolated murine CD8+ T cells with BAY-876 and analyzed markers for T cell activation (CD69 and PD-1), proliferation, cytokine production (TNF-α and IFNγ), and cytotoxicity upon co-culture with tumor cells. Treatment with BAY-876 at a concentration of 200 nM, the same dose used for treating tumor cells *in vitro*, did not affect CD69 expression and proliferation (Figures S6C and S6D). BAY-876 treatment resulted in a slight increase in PD-1 expression in OT-I T cells (Figure S6C). However, cytokine production and target killing ability were comparable between the two groups (Figures S6E and S6F). These data suggest that BAY-876 treatment does not induce a detrimental effect on the activation and cytotoxicity in CD8+ T cells.

The glycolysis pathway level interacts with the TNF-α level to affect patient prognosis in multiple clinical cancer cohorts

We assessed the potential relationship between the glycolysis pathway, TNF-α level, and T cell-mediated anti-tumor immunity in multiple clinical data cohorts. First, we examined the relationship between glycolysis pathway level and the estimated level of T cell infiltrations in bulk tumors. Overall, GLUT1 expression and the glycolysis pathway level were both negatively correlated with CD8+ T cell infiltration, as inferred by EPIC,[36] xCell,[37] and CIBERSORT[38,39] (Figure 7A). To determine the impact of glycolysis on the outcome of ICB treatment, we analyzed 16 published ICB clinical trial datasets and found that in 4 cohorts the expression of glycolysis signature was associated with a better response to ICB (Figures 7B, 7C, and S7A).

Next, we investigated whether the glycolysis pathway level interacts with TNF-α expression level to affect patient survival benefits. For each cancer type in TCGA cohorts, we divided patients into four groups according to the TNF-α expression level and the glycolysis pathway level. We found a total of ten TCGA cohorts, particularly lung adenocarcinoma (LUAD) and PAAD, in which patients with a glycolysis^{low}/TNF-α^{high} signature showed substantial survival benefit as compared with patients with a glycolysis^{high}/TNF-α^{low} signature (Figures 7D and S7B). Similarly, in LUAD and PAAD, GLUT1^{low}/TNF-α^{high} expression profiles were associated with better survival (Figure 7E). We also analyzed potential interaction between glycolysis pathway level and the TNF-α expression level in the context of pre-ICB samples from clinical trials. To this end, we analyzed a metastatic urothelial cancer[40] because of the large cohort size (n = 347) for further stratification into subgroups. We divided the patients into low- and high-glycolysis groups based on the expression level of the glycolysis pathway level. Interestingly, high levels of TNF expression were strongly correlated with survival benefits when the glycolysis signature or GLUT1 expression level was low, but such survival benefits were diminished in patients with high-glycolysis signature or GLUT1 expression level (Figures 7F and 7G). Together, these data suggest that the glycolysis pathway and GLUT1 expression are correlated with TNF-α-mediated anti-tumor activity in human cancers.

DISCUSSION

Resistance to T cell-mediated killing is a major mechanism of immune evasion and resistance to ICB therapies.[41] In this study, we report a novel mechanism by which the tumor-intrinsic glycolysis pathway confers resistance to T cell-mediated killing via TNF-α. TNF-α is a major cytokine released by CTLs and many other types of immune cells, such as macrophages.[42] TNF-α transduces two downstream events that antagonize each other: a pro-survival signal mediated by NF-κB activation and a pro-cell death signal mediated by the

(G–I) LLC cells were pretreated with 200 nM BAY-876 in the presence or absence of 50 μM 2-mercaptoethanol (2-ME) for 24 h, followed by treatment with 20 ng/mL TNF-α for 24 h (G) and 48 h (H and I), respectively. The levels of H2-DCFDA (G) and viable cells (H) were then determined by FACS (n = 4). Cleaved caspase-8 was determined by western blots (I).

Data are represented as mean ± SD (D and H) and mean ± SEM (E and F). **p < 0.01, ***p < 0.001, and ****p < 0.0001 by one-way ANOVA (D and H). ns, not significant. Data are representative of at least two independent experiments (D–I).

Please cite this article in press as: Wu et al., Tumor aerobic glycolysis confers immune evasion through modulating sensitivity to T cell-mediated bystander killing via TNF-α, Cell Metabolism (2023), https://doi.org/10.1016/j.cmet.2023.07.001

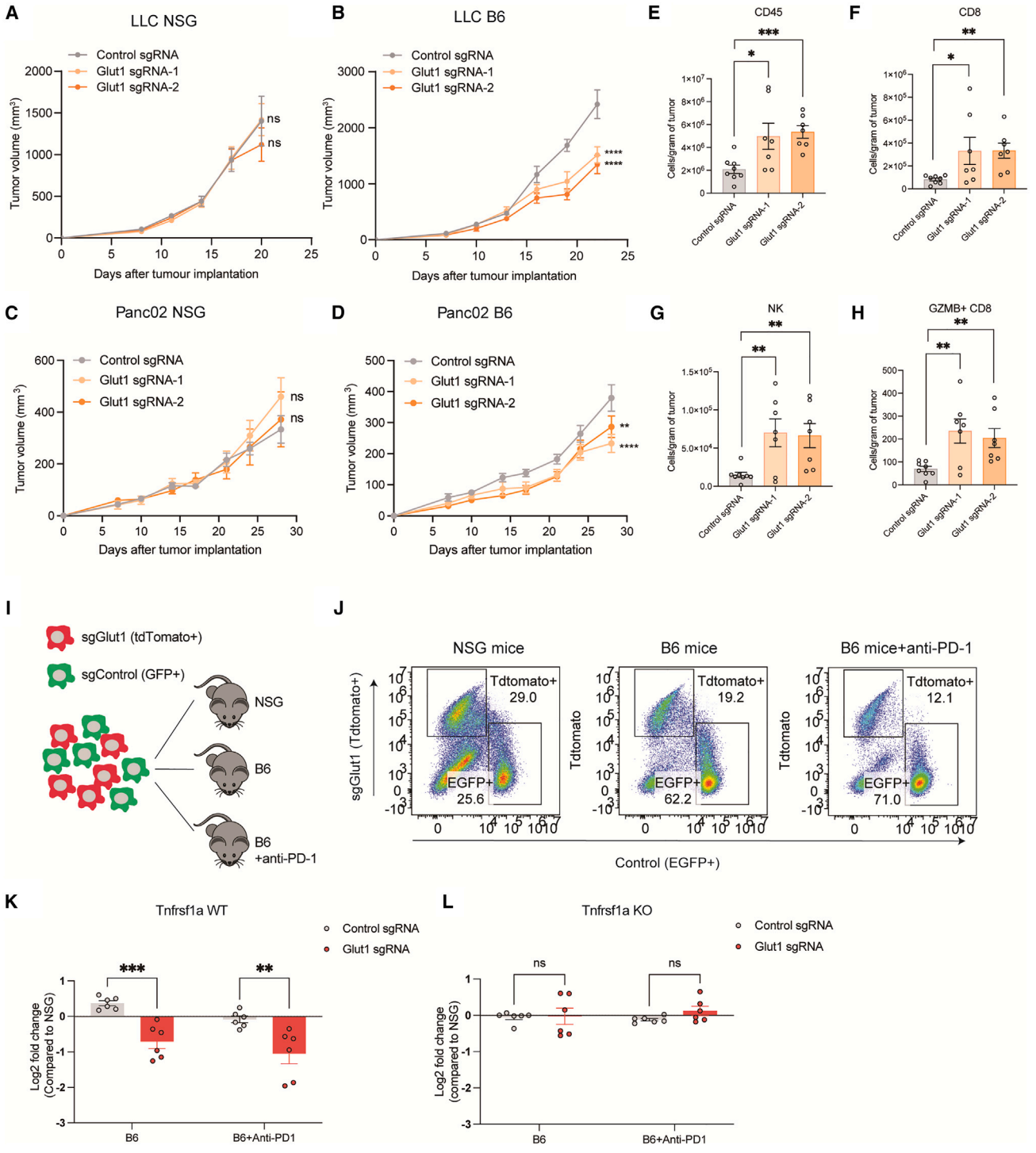

Figure 5. Glut1 KO cells were intrinsically sensitive to anti-tumor immunity mediated by TNF-α

(A and B) Tumor volume of control or Glut1 KO LLC tumors in NSG (A) and wild-type (WT) C57BL/6 mice (B), respectively (n = 6–8).

(C and D) Tumor volume of control or Glut1 KO Panc02 tumors in NSG (C) and wild-type (WT) C57BL/6 mice (D), respectively (n = 4–5).

(E–H) Summary of flow cytometry analysis of the number of infiltrated immune cells in control and Glut1 KO tumors (n = 7–8).

(I) Diagram of *in vivo* competition assay. Mixture of Glut1 KO and control cells (~1:1 ratio) was inoculated in NSG, wild-type mice, and wild-type mice treated with anti-PD-1. The ratio of Glut1 KO and control cells was examined by FACS.

(J) Representative FACS plot showing the ratio change of Glut1 KO cells as compared with control under indicated conditions.

(K) Summary of $\log_2$ fold change of percentages of Glut1 KO cells as compared with control in mice with indicated treatment (n = 6).

(legend continued on next page)

Please cite this article in press as: Wu et al., Tumor aerobic glycolysis confers immune evasion through modulating sensitivity to T cell-mediated bystander killing via TNF-α, Cell Metabolism (2023), https://doi.org/10.1016/j.cmet.2023.07.001

formation of an apoptosis/necrosis complex.[42] Considerable interest has been focused on developing strategies to potentiate TNF-α-induced cell death by perturbing signaling downstream of the TNFR. One such strategy is to block TNF-α-induced NF-κB activation while preserving the formation of apoptosis/necrosis complexes. Studies have shown that genetically targeting complex I components (e.g., RIPK1) and several other components of NF-κB signaling sensitizes tumors to T cell-mediated killing and potentiates anti-tumor immune responses.[9–11,19,25,26] Indeed, the CRISPR screens conducted in this study also revealed that inactivation of NF-κB signaling components sensitized tumors to T cell-mediated killing. However, whether and how other oncogenic pathways interfere with the onset of TNF-α-induced cell death remains unclear. In this regard, we provide evidence that tumor cells with impaired glycolysis are highly sensitive to TNF-α-induced cell death. Mechanistically, inhibition of glycolysis and treatment with TNF-α synergistically resulted in elevated levels of intracellular ROS, which potentiated TNF-α-mediated cell death. This finding is significant because metabolic rewiring toward glycolysis is a hallmark of cancer that is broadly relevant in a wide range of cancer types.[43] We showed that inhibition of Glut1 specifically sensitizes tumors to T cell-mediated killing without affecting cell fitness at baseline. Importantly, GLUT1 is overexpressed in many human cancers as it is a direct downstream target of oncogenic KRAS, which accounts for over 25% of all human cancers.[44] Thus, our study presents GLUT1 as a novel actionable target, whose loss of function sensitizes tumors to TNF-α-mediated cell death.

Our data also shed light on how tumor metabolism affects immune editing, a process that enables tumor cells to escape surveillance by the host immune system.[45] CTL-mediated direct killing through the interaction of TCR and the MHC-peptide complex drives the immune selection of low immunogenic tumors, such as tumors with low levels of MHC-I expression and silenced expression of tumor antigens.[45] What is the potential outcome of immune-editing-driven T cell-mediated bystander killing? We present data suggesting that T cell-mediated bystander killing through TNF-α facilitates the selection of highly glycolytic tumors. By performing *in vivo* competition experiments, we showed that Glut1 KO tumors were strongly selected against only in immune-competent mice, but not in NSG mice. This selection was more evident when the mice were treated with anti-PD-1. Importantly, the relative growth disadvantage of Glut1 KO tumors in immunocompetent mice was completely abolished when the tumor TNFR was inactivated, suggesting that this immune selection was driven by TNF-α. We further showed that the therapeutic effect of the Glut1 inhibitor BAY-876 plus anti-PD-1 was also abolished when tumor-intrinsic TNFR was deleted, indicating that the therapeutic effect of BAY-876 also relies on TNF-α signaling in tumor cells. Based on these data, we propose an immune selection model in which tumors with high glycolysis are favorably selected by the adaptive immune system through TNF-α signaling.

We found a striking difference in the expression patterns of glucose transporters in tumor cells versus immune cells. Consistent with a report,[46] tumor cells showed a preference for GLUT1 expression, whereas immune cells predominantly expressed GLUT3 at elevated levels. Earlier studies have indicated that both GLUT1 and GLUT3 are expressed and functionally important in activated T cells, especially in CD4 T cells.[47–49] Our data show that Glut1 inhibition by BAY-876 had a minimal impact on CD8 T cell activation, proliferation, and tumor killing. In contrast, a prior study showed a marked reduction in CD4 T cell count following BAY-876 treatment.[50] This could suggest a higher dependency of CD4 T cells on GLUT1 for proliferation and effector function, as supported by another study using genetic deletion of GLUT1 in T cells.[47] Interestingly, it has been reported that CD4 and CD8 T cells exhibit different metabolic programs upon activation, with CD8 T cells showing greater resistance to glycolytic inhibition than their CD4 counterparts.[51] Thus, CD4 and CD8 T cells could respond differently upon Glut1 inhibition. Our findings indicate that GLUT1 inhibition can boost anti-tumor immunity through sensitizing tumor cells to TNF-α-induced cell death. Given the essential role of GLUT1 in CD4 T cells, which could release TNF-α, future investigation is needed to evaluate the effect of Glut1 inhibitor in a wider range of tumor models and immune cells in the TME, particularly in those highly infiltrated with CD4 T cells.

When combined with Glut1 inhibition and anti-PD-1 therapy, we observed a striking increase in the infiltration of CD45+ immune cells, including granzyme B+ CTLs and NK cells. The cause of elevated immune cell infiltration in low-glycolysis tumors requires further investigation. One possible mechanism is that low-glycolysis tumors produce less lactate, which is known to be a potent inhibitor of T cell function.[52,53] Another possible mechanism is that Glut1 inhibition alleviates metabolic competition between tumors and T cells.[14] It is also possible that inhibition of glycolysis increases the immunogenicity of tumor cells. For example, a previous study reported that high glycolysis activity inhibits the expression of inflammatory genes and chemokines, such as CXCL10, which is a potent attractor of T cells.[54] These mechanisms could potentially explain the enhanced immune infiltration phenotype in Glut1 KO tumors.

Limitations of the study

In this study, we have shown that Glut1 inhibition potentiates TNF-α-induced apoptosis via ROS. Specifically, we have demonstrated that the protein level of c-FLIP, a major negative regulator of the TNF-α-induced cell death pathway, is downregulated by ROS. However, it remains unclear how ROS regulates c-FLIP at both the transcriptional and post-translational levels. Additionally, it is possible that other regulators of the TNF-α pathway are also modulated by high levels of cellular ROS upon Glut1 inhibition. Therefore, a more comprehensive investigation into the biochemical processes by which ROS regulate TNF-α pathway is necessary in the future.

(L) Summary of log fold change of percentages of Glut1/Tnfrsf1a double KO cells as compared with Tnfrsf1a KO cells in mice with indicated treatment (n = 6). Data are represented as mean ± SEM (A–H, K, and L). *p < 0.05, **p < 0.01, ***p < 0.001, and ****p < 0.0001 by two-way ANOVA (A–D, K, and L) and unpaired Student's t test (E–H). ns, not significant. Data are representative of at least two independent experiments (A–H).

Please cite this article in press as: Wu et al., Tumor aerobic glycolysis confers immune evasion through modulating sensitivity to T cell-mediated bystander killing via TNF-α, Cell Metabolism (2023), https://doi.org/10.1016/j.cmet.2023.07.001

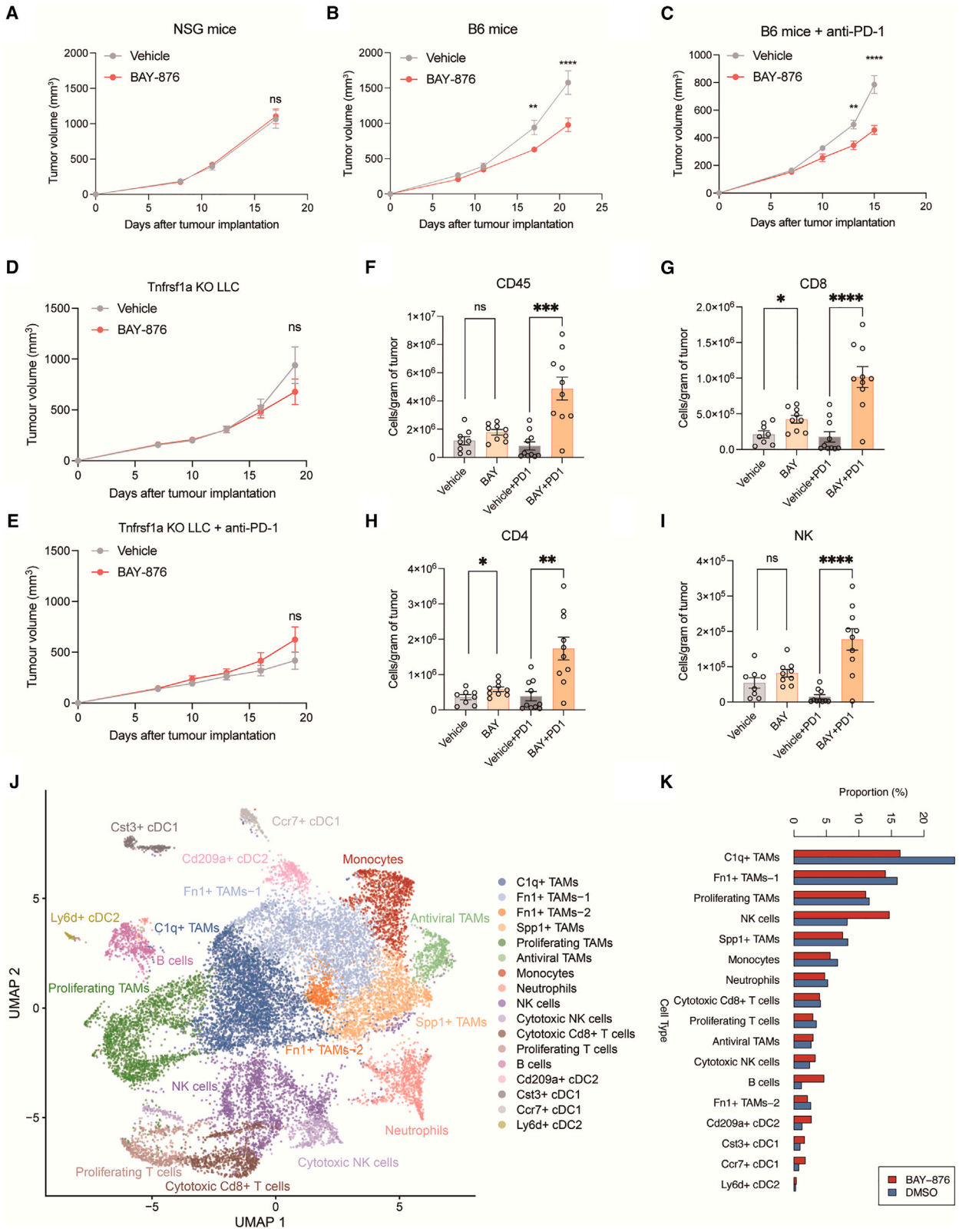

Figure 6. GLUT1 inhibition potentiates anti-tumor immunity and synergizes with immune checkpoint blockades

(A–C) LLC tumor volume following treatment of BAY-876 or vehicle control in NSG (A), wild-type (WT) C57BL/6 mice (B), or C57BL/6 mice treated with anti-PD-1 (C) (n = 6–10).

(legend continued on next page)

STAR★METHODS

Detailed methods are provided in the online version of this paper and include the following:

- KEY RESOURCES TABLE
- RESOURCE AVAILABILITY
  - Lead contact
  - Materials availability
  - Data and code availability
- EXPERIMENTAL MODEL AND SUBJECT DETAILS
  - Cell lines
  - Primary cultures
  - Animal studies
  - Human specimens
- METHOD DETAILS
  - CRISPR screens
  - Data analysis for CRISPR screens
  - Generation of KO cell lines
  - *In vitro* tumor-CTL co-culture and cytokine treatment experiments
  - *In vitro* CTL experiments to determine Glut1 inhibition effects on T cell functions
  - *In vitro* FACS experiments to determine cell apoptosis and ROS level
  - Real time qPCR experiments
  - Cell titer Glo experiments
  - Seahorse experiments
  - Mouse tumor experiments
  - *In vivo* competition experiments
  - Analysis of tumor infiltrating lymphocytes
  - Adoptive transfer experiments
  - Western blot
  - Immunofluorescence staining of human samples
  - Bulk RNA-seq
  - Single cell RNA-seq analysis
  - Single cell analysis for human samples
  - Analysis of ICB cohorts
  - Analysis of TCGA cohorts
- QUANTIFICATION AND STATISTICAL ANALYSIS

SUPPLEMENTAL INFORMATION

Supplemental information can be found online at https://doi.org/10.1016/j.cmet.2023.07.001.

ACKNOWLEDGMENTS

We thank Zimeng Wei for assistance with the experiments. We thank all the members of the Pan and Zeng labs for their comments and suggestions. This work was supported by the Tsinghua-Peking University Center of Life Science (D.P. and Z.Z.), National Science Foundation of China grant 82073163 (D.P.), and Medical Sci-Tech innovation platform of Zhongnan Hospital (PTXM2021001) (F.W.).

AUTHOR CONTRIBUTIONS

Conceptualization, L.W., Z.Z., and D.P.; methodology, L.W. and Y.J.; validation, L.W., Y.J., X.Z., K.T., L.T., Y.Z., K.X., X.Y., and C.L.; investigation, L.W., Y.J., X.Z., T.K., L.T., Y.Z., K.X., X.Y., C.L., and F.W.; formal analysis, L.W., Y.J., X.Z., T.K., L.T., Y.Z., K.X., X.Y., C.L., J.Z., and D.P.; writing – original draft, L.W. and Y.J.; data curation, Y.J., X.Z., and Z.Z.; software, Y.J. and Z.Z.; writing – review & editing, T.K., L.T., Y.Z., K.X., X.Y., C.L., J.Z., Z.Z., and D.P.; resources, F.W.; funding acquisition, Z.Z. and D.P.; supervision, Z.Z. and D.P.; project administration, D.P.

DECLARATION OF INTERESTS

D.P. received sponsored research funding from Bayer AG and Boehringer Ingelheim. These grants were not related to the research reported in this study.

INCLUSION AND DIVERSITY

We support inclusive, diverse, and equitable conduct of research.

Received: November 11, 2022
Revised: May 9, 2023
Accepted: July 2, 2023
Published: July 27, 2023

REFERENCES

1. Zhang, N., and Bevan, M.J. (2011). CD8(+) T cells: foot soldiers of the immune system. Immunity *35*, 161–168. https://doi.org/10.1016/j.immuni.2011.07.010.
2. Voskoboinik, I., Whisstock, J.C., and Trapani, J.A. (2015). Perforin and granzymes: function, dysfunction and human pathology. Nat. Rev. Immunol. *15*, 388–400. https://doi.org/10.1038/nri3839.
3. Zaretsky, J.M., Garcia-Diaz, A., Shin, D.S., Escuin-Ordinas, H., Hugo, W., Hu-Lieskovan, S., Torrejon, D.Y., Abril-Rodriguez, G., Sandoval, S., Barthly, L., et al. (2016). Mutations associated with acquired resistance to PD-1 blockade in melanoma. N. Engl. J. Med. *375*, 819–829. https://doi.org/10.1056/NEJMoa1604958.
4. Sade-Feldman, M., Jiao, Y.J., Chen, J.H., Rooney, M.S., Barzily-Rokni, M., Eliane, J.P., Bjorgaard, S.L., Hammond, M.R., Vitzthum, H., Blackmon, S.M., et al. (2017). Resistance to checkpoint blockade therapy through inactivation of antigen presentation. Nat. Commun. *8*, 1136. https://doi.org/10.1038/s41467-017-01062-w.
5. Jiang, P., Gu, S., Pan, D., Fu, J., Sahu, A., Hu, X., Li, Z., Traugh, N., Bu, X., Li, B., et al. (2018). Signatures of T cell dysfunction and exclusion predict cancer immunotherapy response. Nat. Med. *24*, 1550–1558. https://doi.org/10.1038/s41591-018-0136-1.
6. Juneja, V.R., McGuire, K.A., Manguso, R.T., LaFleur, M.W., Collins, N., Haining, W.N., Freeman, G.J., and Sharpe, A.H. (2017). PD-L1 on tumor cells is sufficient for immune evasion in immunogenic tumors and inhibits CD8 T cell cytotoxicity. J. Exp. Med. *214*, 895–904. https://doi.org/10.1084/jem.20160801.
7. Annibaldi, A., and Meier, P. (2018). Checkpoints in TNF-induced cell death: implications in inflammation and cancer. Trends Mol. Med. *24*, 49–65. https://doi.org/10.1016/j.molmed.2017.11.002.

(D and E) Tumor volume of Tnfrsf1a KO LLC tumors following treatment of BAY-876 or vehicle control in C57BL/6 mice (D) or C57BL/6 mice treated with anti-PD-1 (E) (n = 7–8).
(F–I) Summary of flow cytometry analysis of the number of infiltrated immune cells following indicated treatment (n = 8–10).
(J) UMAP plot of cells from scRNA-seq from LLC tumors following treatment of BAY-876 and vehicle control.
(K) Relative percentage of immune populations in scRNA-seq from LLC tumors following treatment of BAY-876 and vehicle control.
Data are represented as mean ± SEM (A–I). *p < 0.05, **p < 0.01, ***p < 0.001, and ****p < 0.0001 by two-way ANOVA (A–E) and unpaired Student's t test (F–I). ns, not significant. Data are representative of at least two independent experiments (A–I).

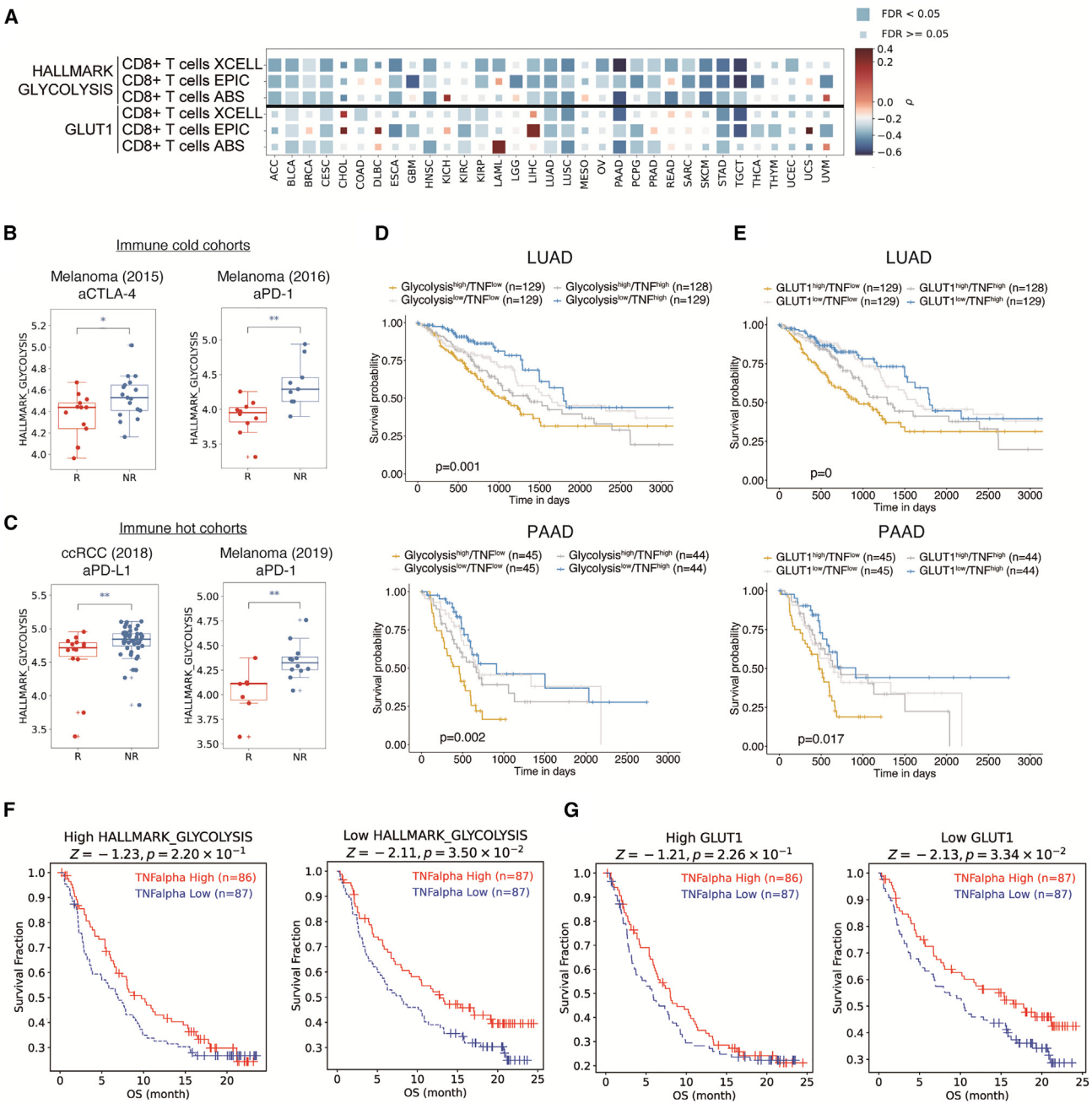

Figure 7. Clinical relevance for targeting glycolysis pathway to enhance anti-tumor immunity

(A) Heatmap showing Spearman correlations between CD8+ T cells infiltration and GSVA score of indicated gene sets in each TCGA cohort.

(B and C) HALLMARK_GLYCOLYSIS expression level of the responders and non-responders of representative immune-cold (B) and -hot (C) cohorts.

(D) Overall survival of TCGA cohorts (LUAD and PAAD) based on the level of HALLMARK_GLYCOLYSIS and TNF-α.

(E) Overall survival of TCGA cohorts (LUAD and PAAD) based on the level of GLUT1 and TNF-α.

(F and G) Overall survival of an ICB cohort[40] based on the level of HALLMARK_GLYCOLYSIS and TNF-α (F) or the level of GLUT1 and TNF-α (G).

*p < 0.05, **p < 0.01 by linear regression model (B and C).

8. Young, T.M., Reyes, C., Pasnikowski, E., Castanaro, C., Wong, C., Decker, C.E., Chiu, J., Song, H., Wei, Y., Bai, Y., et al. (2020). Autophagy protects tumors from T cell-mediated cytotoxicity via inhibition of TNFalpha-induced apoptosis. Sci. Immunol. *5*. https://doi.org/10.1126/sciimmunol.abb9561.

9. Cucolo, L., Chen, Q., Qiu, J., Yu, Y., Klapholz, M., Budinich, K.A., Zhang, Z., Shao, Y., Brodsky, I.E., Jordan, M.S., et al. (2022). The interferon-stimulated gene RIPK1 regulates cancer cell intrinsic and extrinsic resistance to immune checkpoint blockade. Immunity *55*, 671–685.e10. https://doi.org/10.1016/j.immuni.2022.03.007.

10. Frey, N., Tortola, L., Egli, D., Janjuha, S., Rothgangl, T., Marquart, K.F., Ampenberger, F., Kopf, M., and Schwank, G. (2022). Loss of Rnf31 and Vps4b sensitizes pancreatic cancer to T cell-mediated killing. Nat. Commun. *13*, 1804. https://doi.org/10.1038/s41467-022-29412-3.

11. Vredevoogd, D.W., Kuilman, T., Ligtenberg, M.A., Boshuizen, J., Stecker, K.E., de Bruijn, B., Krijgsman, O., Huang, X., Kenski, J.C.N., Lacroix, R., et al. (2020). Augmenting immunotherapy impact by lowering tumor TNF cytotoxicity threshold. Cell *180*, 404–405. https://doi.org/10.1016/j.cell.2020.01.005.

12. Zhang, Z., Kong, X., Ligtenberg, M.A., van Hal-van Veen, S.E., Visser, N.L., de Bruijn, B., Stecker, K., van der Helm, P.W., Kuilman, T., Hoefsmit, E.P., et al. (2022). RNF31 inhibition sensitizes tumors to bystander killing by innate and adaptive immune cells. Cell Rep. Med. *3*, 100655. https://doi.org/10.1016/j.xcrm.2022.100655.

13. Hanahan, D. (2022). Hallmarks of cancer: new dimensions. Cancer Discov. *12*, 31–46. https://doi.org/10.1158/2159-8290.CD-21-1059.

14. Chang, C.H., Qiu, J., O'Sullivan, D., Buck, M.D., Noguchi, T., Curtis, J.D., Chen, Q., Gindin, M., Gubin, M.M., van der Windt, G.J., et al. (2015). Metabolic competition in the tumor microenvironment is a driver of cancer progression. Cell *162*, 1229–1241. https://doi.org/10.1016/j.cell.2015.08.016.

15. Buck, M.D., Sowell, R.T., Kaech, S.M., and Pearce, E.L. (2017). Metabolic instruction of immunity. Cell *169*, 570–586. https://doi.org/10.1016/j.cell.2017.04.004.

16. Quinn, W.J., 3rd, Jiao, J., TeSlaa, T., Stadanlick, J., Wang, Z., Wang, L., Akimova, T., Angelin, A., Schäfer, P.M., Cully, M.D., et al. (2020). Lactate limits T cell proliferation via the NAD(H) redox state. Cell Rep. *33*, 108500. https://doi.org/10.1016/j.celrep.2020.108500.

17. Cascone, T., McKenzie, J.A., Mbofung, R.M., Punt, S., Wang, Z., Xu, C., Williams, L.J., Wang, Z., Bristow, C.A., Carugo, A., et al. (2018). Increased tumor glycolysis characterizes immune resistance to adoptive T cell therapy. Cell Metab. *27*, 977–987.e4. https://doi.org/10.1016/j.cmet.2018.02.024.

18. Guo, D., Tong, Y., Jiang, X., Meng, Y., Jiang, H., Du, L., Wu, Q., Li, S., Luo, S., Li, M., et al. (2022). Aerobic glycolysis promotes tumor immune evasion by hexokinase2-mediated phosphorylation of IκBα. Cell Metab. *34*, 1312–1324.e6. https://doi.org/10.1016/j.cmet.2022.08.002.

19. Pan, D., Kobayashi, A., Jiang, P., Ferrari de Andrade, L., Tay, R.E., Luoma, A.M., Tsoucas, D., Qiu, X., Lim, K., Rao, P., et al. (2018). A major chromatin regulator determines resistance of tumor cells to T cell-mediated killing. Science *359*, 770–775. https://doi.org/10.1126/science.aao1710.

20. Lawson, K.A., Sousa, C.M., Zhang, X., Kim, E., Akthar, R., Caumanns, J.J., Yao, Y., Mikolajewicz, N., Ross, C., Brown, K.R., et al. (2020). Functional genomic landscape of cancer-intrinsic evasion of killing by T cells. Nature *586*, 120–126. https://doi.org/10.1038/s41586-020-2746-2.

21. Stine, Z.E., Schug, Z.T., Salvino, J.M., and Dang, C.V. (2022). Targeting cancer metabolism in the era of precision oncology. Nat. Rev. Drug Discov. *21*, 141–162. https://doi.org/10.1038/s41573-021-00339-6.

22. Siebeneicher, H., Cleve, A., Rehwinkel, H., Neuhaus, R., Heisler, I., Müller, T., Bauser, M., and Buchmann, B. (2016). Identification and optimization of the first highly selective GLUT1 inhibitor BAY-876. ChemMedChem *11*, 2261–2271. https://doi.org/10.1002/cmdc.201600276.

23. Peng, M., Yin, N., Chhangawala, S., Xu, K., Leslie, C.S., and Li, M.O. (2016). Aerobic glycolysis promotes T helper 1 cell differentiation through an epigenetic mechanism. Science *354*, 481–484. https://doi.org/10.1126/science.aaf6284.

24. Thorens, B., and Mueckler, M. (2010). Glucose transporters in the 21st Century. Am. J. Physiol. Endocrinol. Metab. *298*, E141–E145. https://doi.org/10.1152/ajpendo.00712.2009.

25. Manguso, R.T., Pope, H.W., Zimmer, M.D., Brown, F.D., Yates, K.B., Miller, B.C., Collins, N.B., Bi, K., LaFleur, M.W., Juneja, V.R., et al. (2017). In vivo CRISPR screening identifies Ptpn2 as a cancer immunotherapy target. Nature *547*, 413–418. https://doi.org/10.1038/nature23270.

26. Kearney, C.J., Vervoort, S.J., Hogg, S.J., Ramsbottom, K.M., Freeman, A.J., Lalaoui, N., Pijpers, L., Michie, J., Brown, K.K., Knight, D.A., et al. (2018). Tumor immune evasion arises through loss of TNF sensitivity. Sci. Immunol. *3*. https://doi.org/10.1126/sciimmunol.aar3451.

27. Qin, Q., Fan, J., Zheng, R., Wan, C., Mei, S., Wu, Q., Sun, H., Brown, M., Zhang, J., Meyer, C.A., et al. (2020). Lisa: inferring transcriptional regulators through integrative modeling of public chromatin accessibility and ChIP-seq data. Genome Biol. *21*, 32. https://doi.org/10.1186/s13059-020-1934-6.

28. Lange, P.S., Chavez, J.C., Pinto, J.T., Coppola, G., Sun, C.W., Townes, T.M., Geschwind, D.H., and Ratan, R.R. (2008). ATF4 is an oxidative stress-inducible, prodeath transcription factor in neurons in vitro and in vivo. J. Exp. Med. *205*, 1227–1242. https://doi.org/10.1084/jem.20071460.

29. Han, J., Back, S.H., Hur, J., Lin, Y.H., Gildersleeve, R., Shan, J.X., Yuan, C.L., Krokowski, D., Wang, S.Y., Hatzoglou, M., et al. (2013). ER-stress-induced transcriptional regulation increases protein synthesis leading to cell death. Nat. Cell Biol. *15*, 481–490. https://doi.org/10.1038/ncb2738.

30. Marciniak, S.J., Yun, C.Y., Oyadomari, S., Novoa, I., Zhang, Y.H., Jungreis, R., Nagata, K., Harding, H.P., and Ron, D. (2004). CHOP induces death by promoting protein synthesis and oxidation in the stressed endoplasmic reticulum. Genes Dev. *18*, 3066–3077. https://doi.org/10.1101/gad.1250704.

31. Kim, J.J., Lee, S.B., Park, J.K., and Yoo, Y.D. (2010). TNF-alpha-induced ROS production triggering apoptosis is directly linked to Romo1 and Bcl-X(L). Cell Death Differ. *17*, 1420–1434. https://doi.org/10.1038/cdd.2010.19.

32. Zhang, Y., Su, S.S., Zhao, S., Yang, Z., Zhong, C.Q., Chen, X., Cai, Q., Yang, Z.H., Huang, D., Wu, R., et al. (2017). RIP1 autophosphorylation is promoted by mitochondrial ROS and is essential for RIP3 recruitment into necrosome. Nat. Commun. *8*, 14329. https://doi.org/10.1038/ncomms14329.

33. Zhang, D.W., Shao, J., Lin, J., Zhang, N., Lu, B.J., Lin, S.C., Dong, M.Q., and Han, J. (2009). RIP3, an energy metabolism regulator that switches TNF-induced cell death from apoptosis to necrosis. Science *325*, 332–336. https://doi.org/10.1126/science.1172308.

34. Wang, P.X., Ji, Y.X., Zhang, X.J., Zhao, L.P., Yan, Z.Z., Zhang, P., Shen, L.J., Yang, X., Fang, J., Tian, S., et al. (2017). Targeting CASP8 and FADD-like apoptosis regulator ameliorates nonalcoholic steatohepatitis in mice and nonhuman primates. Nat. Med. *23*, 439–449. https://doi.org/10.1038/nm.4290.

35. Du, J., Wu, J., Fu, X., Tse, A.K., Li, T., Su, T., and Yu, Z.L. (2016). Icariside II overcomes TRAIL resistance of melanoma cells through ROS-mediated downregulation of STAT3/cFLIP signaling. Oncotarget *7*, 52218–52229. https://doi.org/10.18632/oncotarget.10582.

36. Racle, J., de Jonge, K., Baumgaertner, P., Speiser, D.E., and Gfeller, D. (2017). Simultaneous enumeration of cancer and immune cell types from bulk tumor gene expression data. eLife *6*, e26476. https://doi.org/10.7554/eLife.26476.

37. Aran, D., Hu, Z., and Butte, A.J. (2017). xCell: digitally portraying the tissue cellular heterogeneity landscape. Genome Biol. *18*, 220. https://doi.org/10.1186/s13059-017-1349-1.

38. Newman, A.M., Liu, C.L., Green, M.R., Gentles, A.J., Feng, W., Xu, Y., Hoang, C.D., Diehn, M., and Alizadeh, A.A. (2015). Robust enumeration of cell subsets from tissue expression profiles. Nat. Methods *12*, 453–457. https://doi.org/10.1038/nmeth.3337.

39. Chen, B., Khodadoust, M.S., Liu, C.L., Newman, A.M., and Alizadeh, A.A. (2018). Profiling tumor infiltrating immune cells with CIBERSORT. Methods Mol. Biol. *1711*, 243–259. https://doi.org/10.1007/978-1-4939-7493-1_12.

40. Mariathasan, S., Turley, S.J., Nickles, D., Castiglioni, A., Yuen, K., Wang, Y., Kadel, E.E., III, Koeppen, H., Astarita, J.L., Cubas, R., et al. (2018). TGFbeta attenuates tumour response to PD-L1 blockade by contributing to exclusion of T cells. Nature *554*, 544–548. https://doi.org/10.1038/nature25501.

41. Kalbasi, A., and Ribas, A. (2020). Tumour-intrinsic resistance to immune checkpoint blockade. Nat. Rev. Immunol. *20*, 25–39. https://doi.org/10.1038/s41577-019-0218-4.

42. Croft, M. (2009). The role of TNF superfamily members in T-cell function and diseases. Nat. Rev. Immunol. *9*, 271–285. https://doi.org/10.1038/nri2526.

43. Hanahan, D., and Weinberg, R.A. (2011). Hallmarks of cancer: the next generation. Cell *144*, 646–674. https://doi.org/10.1016/j.cell.2011.02.013.

44. Yun, J., Rago, C., Cheong, I., Pagliarini, R., Angenendt, P., Rajagopalan, H., Schmidt, K., Willson, J.K., Markowitz, S., Zhou, S., et al. (2009). Glucose deprivation contributes to the development of KRAS pathway mutations in tumor cells. Science *325*, 1555–1559. https://doi.org/10.1126/science.1174229.

45. Vesely, M.D., and Schreiber, R.D. (2013). Cancer immunoediting: antigens, mechanisms, and implications to cancer immunotherapy. Ann. NY Acad. Sci. *1284*, 1–5. https://doi.org/10.1111/nyas.12105.

46. Na, K.J., Choi, H., Oh, H.R., Kim, Y.H., Lee, S.B., Jung, Y.J., Koh, J., Park, S., Lee, H.J., Jeon, Y.K., et al. (2020). Reciprocal change in glucose metabolism of cancer and immune cells mediated by different glucose transporters predicts immunotherapy response. Theranostics *10*, 9579–9590. https://doi.org/10.7150/thno.48954.

47. Macintyre, A.N., Gerriets, V.A., Nichols, A.G., Michalek, R.D., Rudolph, M.C., Deoliveira, D., Anderson, S.M., Abel, E.D., Chen, B.J., Hale, L.P., et al. (2014). The glucose transporter Glut1 is selectively essential for CD4 T cell activation and effector function. Cell Metab. *20*, 61–72. https://doi.org/10.1016/j.cmet.2014.05.004.

48. Hochrein, S.M., Wu, H., Eckstein, M., Arrigoni, L., Herman, J.S., Schumacher, F., Gerecke, C., Rosenfeldt, M., Grün, D., Kleuser, B., et al. (2022). The glucose transporter GLUT3 controls T helper 17 cell responses through glycolytic-epigenetic reprogramming. Cell Metab. *34*, 516–532.e11. https://doi.org/10.1016/j.cmet.2022.02.015.

49. Beckermann, K.E., Hongo, R., Ye, X., Young, K., Carbonell, K., Healey, D.C.C., Siska, P.J., Barone, S., Roe, C.E., Smith, C.C., et al. (2020). CD28 costimulation drives tumor-infiltrating T cell glycolysis to promote inflammation. JCI Insight *5*. https://doi.org/10.1172/jci.insight.138729.

50. Chen, Z., Vaeth, M., Eckstein, M., Delgobo, M., Ramos, G., Frantz, S., Hofmann, U., and Gladow, N. (2023). Characterization of the effect of the GLUT-1 inhibitor BAY-876 on T cells and macrophages. Eur. J. Pharmacol. *945*, 175552. https://doi.org/10.1016/j.ejphar.2023.175552.

51. Cao, Y., Rathmell, J.C., and Macintyre, A.N. (2014). Metabolic reprogramming towards aerobic glycolysis correlates with greater proliferative ability and resistance to metabolic inhibition in CD8 versus CD4 T cells. PLoS One *9*, e104104. https://doi.org/10.1371/journal.pone.0104104.

52. Brand, A., Singer, K., Koehl, G.E., Kolitzus, M., Schoenhammer, G., Thiel, A., Matos, C., Bruss, C., Klobuch, S., Peter, K., et al. (2016). LDHA-associated lactic acid production blunts tumor immunosurveillance by T and NK cells. Cell Metab. *24*, 657–671. https://doi.org/10.1016/j.cmet.2016.08.011.

53. Elia, I., Rowe, J.H., Johnson, S., Joshi, S., Notarangelo, G., Kurmi, K., Weiss, S., Freeman, G.J., Sharpe, A.H., and Haigis, M.C. (2022). Tumor cells dictate anti-tumor immune responses by altering pyruvate utilization and succinate signaling in CD8(+) T cells. Cell Metab. *34*, 1137–1150.e6. https://doi.org/10.1016/j.cmet.2022.06.008.

54. Karin, N., and Razon, H. (2018). Chemokines beyond chemo-attraction: CXCL10 and its significant role in cancer and autoimmunity. Cytokine *109*, 24–28. https://doi.org/10.1016/j.cyto.2018.02.012.

55. Lambrechts, D., Wauters, E., Boeckx, B., Aibar, S., Nittner, D., Burton, O., Bassez, A., Decaluwé, H., Pircher, A., Van den Eynde, K., et al. (2018). Phenotype molding of stromal cells in the lung tumor microenvironment. Nat. Med. *24*, 1277–1289. https://doi.org/10.1038/s41591-018-0096-5.

56. Song, Q., Hawkins, G.A., Wudel, L., Chou, P.C., Forbes, E., Pullikuth, A.K., Liu, L., Jin, G., Craddock, L., Topaloglu, U., et al. (2019). Dissecting intratumoral myeloid cell plasticity by single cell RNA-seq. Cancer Med. *8*, 3072–3085. https://doi.org/10.1002/cam4.2113.

57. Zilionis, R., Engblom, C., Pfirschke, C., Savova, V., Zemmour, D., Saatcioglu, H.D., Krishnan, I., Maroni, G., Meyerovitz, C.V., Kerwin, C.M., et al. (2019). Single-cell transcriptomics of human and mouse lung cancers reveals conserved myeloid populations across individuals and species. Immunity *50*, 1317–1334.e10. https://doi.org/10.1016/j.immuni.2019.03.009.

58. Chi, Y., Remsik, J., Kiseliovas, V., Derderian, C., Sener, U., Alghader, M., Saadeh, F., Nikishina, K., Bale, T., Iacobuzio-Donahue, C., et al. (2020). Cancer cells deploy lipocalin-2 to collect limiting iron in leptomeningeal metastasis. Science *369*, 276–282. https://doi.org/10.1126/science.aaz2193.

59. Peng, J., Sun, B.F., Chen, C.Y., Zhou, J.Y., Chen, Y.S., Chen, H., Liu, L., Huang, D., Jiang, J., Cui, G.S., et al. (2019). Single-cell RNA-seq highlights intra-tumoral heterogeneity and malignant progression in pancreatic ductal adenocarcinoma. Cell Res. *29*, 725–738. https://doi.org/10.1038/s41422-019-0195-y.

60. Moncada, R., Barkley, D., Wagner, F., Chiodin, M., Devlin, J.C., Baron, M., Hajdu, C.H., Simeone, D.M., and Yanai, I. (2020). Integrating microarray-based spatial transcriptomics and single-cell RNA-seq reveals tissue architecture in pancreatic ductal adenocarcinomas. Nat. Biotechnol. *38*, 333–342. https://doi.org/10.1038/s41587-019-0392-8.

61. Schlesinger, Y., Yosefov-Levi, O., Kolodkin-Gal, D., Granit, R.Z., Peters, L., Kalifa, R., Xia, L., Nasereddin, A., Shiff, I., Amran, O., et al. (2020). Single-cell transcriptomes of pancreatic preinvasive lesions and cancer reveal acinar metaplastic cells' heterogeneity. Nat. Commun. *11*, 4516. https://doi.org/10.1038/s41467-020-18207-z.

62. Lin, W., Noel, P., Borazanci, E.H., Lee, J., Amini, A., Han, I.W., Heo, J.S., Jameson, G.S., Fraser, C., Steinbach, M., et al. (2020). Single-cell transcriptome analysis of tumor and stromal compartments of pancreatic ductal adenocarcinoma primary tumors and metastatic lesions. Genome Med. *12*, 80. https://doi.org/10.1186/s13073-020-00776-9.

63. Chung, W., Eum, H.H., Lee, H.O., Lee, K.M., Lee, H.B., Kim, K.T., Ryu, H.S., Kim, S., Lee, J.E., Park, Y.H., et al. (2017). Single-cell RNA-seq enables comprehensive tumour and immune cell profiling in primary breast cancer. Nat. Commun. *8*, 15081. https://doi.org/10.1038/ncomms15081.

64. Dobin, A., Davis, C.A., Schlesinger, F., Drenkow, J., Zaleski, C., Jha, S., Batut, P., Chaisson, M., and Gingeras, T.R. (2013). STAR: ultrafast universal RNA-seq aligner. Bioinformatics *29*, 15–21. https://doi.org/10.1093/bioinformatics/bts635.

65. Li, W., Xu, H., Xiao, T., Cong, L., Love, M.I., Zhang, F., Irizarry, R.A., Liu, J.S., Brown, M., and Liu, X.S. (2014). MAGeCK enables robust identification of essential genes from genome-scale CRISPR/Cas9 knockout screens. Genome Biol. *15*, 554. https://doi.org/10.1186/s13059-014-0554-4.

66. Stuart, T., Stuart, T., Butler, A., Hoffman, P., Hafemeister, C., Papalexi, E., Mauck, W.M., 3rd, Hao, Y., Stoeckius, M., Smibert, P., and Satija, R. (2019). Comprehensive integration of single-cell data. Cell *177*, 1888–1902.e21. https://doi.org/10.1016/j.cell.2019.05.031.

67. Miao, D., Margolis, C.A., Gao, W., Voss, M.H., Li, W., Martini, D.J., Norton, C., Bossé, D., Wankowicz, S.M., Cullen, D., et al. (2018). Genomic correlates of response to immune checkpoint therapies in clear cell renal cell carcinoma. Science *359*, 801–806.

68. Van Allen, E.M., Miao, D., Schilling, B., Shukla, S.A., Blank, C., Zimmer, L., Sucker, A., Hillen, U., Foppen, M.H.G., Goldinger, S.M., et al. (2015). Genomic correlates of response to CTLA-4 blockade in metastatic melanoma. Science *350*, 207–211.

69. Gide, T.N., Quek, C., Menzies, A.M., Tasker, A.T., Shang, P., Holst, J., Madore, J., Lim, S.Y., Velickovic, R., Wongchenko, M., et al. (2019). Distinct immune cell populations define response to anti-PD-1 monotherapy and anti-PD-1/anti-CTLA-4 combined therapy. Cancer Cell *35*, 238–255.e6.

70. McDermott, D.F., Huseni, M.A., Atkins, M.B., Motzer, R.J., Rini, B.I., Escudier, B., Fong, L., Joseph, R.W., Pal, S.K., Reeves, J.A., et al. (2018). Clinical activity and molecular correlates of response to

atezolizumab alone or in combination with bevacizumab versus sunitinib in renal cell carcinoma. Nat. Med. *24*, 749–757.

71. Zhao, J., Chen, A.X., Gartrell, R.D., Silverman, A.M., Aparicio, L., Chu, T., Bordbar, D., Shan, D., Samanamud, J., Mahajan, A., et al. (2019). Immune and genomic correlates of response to anti-PD-1 immunotherapy in glioblastoma. Nat. Med. *25*, 462–469.

72. Liu, D., Schilling, B., Liu, D., Sucker, A., Livingstone, E., Jerby-Arnon, L., Zimmer, L., Gutzmer, R., Satzger, I., Loquai, C., et al. (2019). Integrative molecular and clinical modeling of clinical outcomes to PD1 blockade in patients with metastatic melanoma. Nat. Med. *25*, 1916–1927.

73. Hugo, W., Zaretsky, J.M., Sun, L., Song, C., Moreno, B.H., Hu-Lieskovan, S., Berent-Maoz, B., Pang, J., Chmielowski, B., Cherry, G., et al. (2016). Genomic and transcriptomic features of response to anti-PD-1 therapy in metastatic melanoma. Cell *165*, 35–44.

74. Riaz, N., Havel, J.J., Makarov, V., Desrichard, A., Urba, W.J., Sims, J.S., Hodi, F.S., Martín-Algarra, S., Mandal, R., Sharfman, W.H., et al. (2017). Tumor and microenvironment evolution during immunotherapy with nivolumab. Cell *171*, 934–949.e16.

75. Kim, S.T., Cristescu, R., Bass, A.J., Kim, K.M., Odegaard, J.I., Kim, K., Liu, X.Q., Sher, X., Jung, H., Lee, M., et al. (2018). Comprehensive molecular characterization of clinical responses to PD-1 inhibition in metastatic gastric cancer. Nat. Med. *24*, 1449–1458.

76. Nathanson, T., Ahuja, A., Rubinsteyn, A., Aksoy, B.A., Hellmann, M.D., Miao, D., Van Allen, E., Merghoub, T., Wolchok, J.D., Snyder, A., et al. (2017). Somatic mutations and neoepitope homology in melanomas treated with CTLA-4 blockade. Cancer Immunol. Res. *5*, 84–91. https://doi.org/10.1158/2326-6066.CIR-16-0019.

77. Uppaluri, R., Campbell, K.M., Egloff, A.M., Zolkind, P., Skidmore, Z.L., Nussenbaum, B., Paniello, R.C., Rich, J.T., Jackson, R., Pipkorn, P., et al. (2020). Neoadjuvant and adjuvant pembrolizumab in resectable locally advanced, human papillomavirus-unrelated head and neck cancer: A multicenter, Phase II trial. Clin. Cancer Res. *26*, 5140–5152. https://doi.org/10.1158/1078-0432.CCR-20-1695.

78. Lee, J.S., Nair, N.U., Dinstag, G., Chapman, L., Chung, Y., Wang, K., Sinha, S., Cha, H., Kim, D., Schperberg, A.V., et al. (2021). Synthetic lethality-mediated precision oncology via the tumor transcriptome. Cell *184*, 2487–2502.e13. https://doi.org/10.1016/j.cell.2021.03.030.

Please cite this article in press as: Wu et al., Tumor aerobic glycolysis confers immune evasion through modulating sensitivity to T cell-mediated bystander killing via TNF-α, Cell Metabolism (2023), https://doi.org/10.1016/j.cmet.2023.07.001

STAR★METHODS

KEY RESOURCES TABLE

REAGENT or RESOURCE	SOURCE	IDENTIFIER
Antibodies		
InVivoPlus anti-mouse CD3ε	Bio X Cell	Cat#BE0001-1; RRID: AB_1107634
InVivoMab anti-mouse CD28	Bio X Cell	Cat# BE0015-1; RRID: AB_1107624
InVivoPlus anti-mouse PD-1 (CD279)	Bio X Cell	Cat#BE0273; RRID: AB_2687796
PE anti-mouse/human CD11b Antibody	Biolegend	Cat#101207; RRID: AB_312790
Brilliant Violet 421 anti-mouse CD11c Antibody	Biolegend	Cat#117329; RRID: AB_10897814
PE anti-mouse CD120a (TNF R Type I/p55) Antibody	Biolegend	Cat#113004; RRID: AB_313533
FITC anti-mouse CD3 Antibody	Biolegend	Cat#100204; RRID: AB_312661
PE anti-mouse CD3 Antibody	Biolegend	Cat#100205; RRID: AB_312662
Brilliant Violet 510 anti-mouse CD4 Antibody	Biolegend	Cat#100559; RRID: AB_2562608
APC anti-mouse CD45 Recombinant Antibody	Biolegend	Cat#157605; RRID: AB_2876537
Brilliant Violet 421 anti-mouse CD45 Antibody	Biolegend	Cat#103133; RRID: AB_10899570
FITC anti-mouse CD45 Antibody	Biolegend	Cat#103107; RRID: AB_312972
Brilliant Violet 510 anti-mouse/human CD45R/B220 Antibody	Biolegend	Cat#103247; RRID: AB_2561394
Brilliant Violet 510 anti-mouse CD69 Antibody	Biolegend	Cat#104531, RRID: AB_2562326
PE anti-mouse CD8a Antibody	Biolegend	Cat#100707, RRID: AB_312746
PE/Cyanine7 anti-mouse CD8a Antibody	Biolegend	Cat#100721; RRID: AB_312760
APC anti-mouse F4/80 Antibody	Biolegend	Cat#123115; RRID: AB_893493
PE/Cyanine7 anti-human/mouse Granzyme B Recombinant Antibody	Biolegend	Cat#372214; RRID: AB_2728381
APC anti-mouse IFN-γ Antibody	Biolegend	Cat#505809; RRID: AB_315403
PE/Cyanine7 anti-mouse I-A/I-E Antibody	Biolegend	Cat#107629; RRID: AB_2290801
Brilliant Violet 510 anti-mouse Ly-6G/Ly-6C (Gr-1) Antibody	Biolegend	Cat#108437; RRID: AB_2562214
FITC anti-mouse TNF-α Antibody	Biolegend	Cat#506303; RRID: AB_315424
TruStain FcX (anti-mouse CD16/32) Antibody	Biolegend	Cat#101320; RRID: AB_1574975
NK1.1 Monoclonal Antibody (PK136), APC	Invitrogen	Cat#17-5941-81; RRID: AB_469478
Cleaved Caspase-8 (Asp387) (D5B2) XP Rabbit mAb	Cell Signaling Technology	Cat#8592; RRID: AB_10891784
Anti-rabbit IgG (H+L), F(ab')$_2$ Fragment (Alexa Fluor 488 Conjugate)	Cell Signaling Technology	Cat#4412; RRID: AB_1904025
Anti-rabbit IgG, HRP-linked Antibody	Cell Signaling Technology	Cat#7074; RRID: AB_2099233
Cleaved Caspase-8 (Asp387) Antibody	Cell Signaling Technology	Cat# 9429; RRID: AB_2068300
β-Tubulin (9F3) Rabbit mAb	Cell Signaling Technology	Cat#2128; RRID: AB_823664
Recombinant Anti-Glucose Transporter GLUT1 antibody	Abcam	Cat#ab115730; RRID: AB_10903230
GPI Polyclonal Antibody	Invitrogen	Cat#PA5-26787; RRID: AB_2544287
Anti-Ki67 antibody	Abcam	Cat#ab15580; RRID: AB_443209
Anti-CD45 Rabbit pAb	Servicebio	Cat#GB113885

(*Continued on next page*)

Please cite this article in press as: Wu et al., Tumor aerobic glycolysis confers immune evasion through modulating sensitivity to T cell-mediated bystander killing via TNF-α, Cell Metabolism (2023), https://doi.org/10.1016/j.cmet.2023.07.001

Continued

REAGENT or RESOURCE	SOURCE	IDENTIFIER
FLIP (D5J1E) Rabbit mAB	Cell Signaling Technology	Cat# 56343, RRID: AB_2799508
Bacterial and virus strains		
Stbl3 Competent Cell	AlpaLife	Cat#KTSM110
Biological samples		
Paraffin-embedded tissue samples, see Table S1	Zhongnan Hospital of Wuhan University	N/A
Chemicals, peptides, and recombinant proteins		
Dulbecco's Modified Eagle Medium (DMEM) basic (1X)	Gibco	Cat#C11995500BT
Roswell Park Memorial Institute (RPMI) 1640 basic (1X)	Gibco	Cat# C11875500BT
Fetal Bovine Serum (FBS)	Biological Industries	Cat#04-001-1ACS
Horse serum	Gibco	Cat# 26050-070
Penicillin-Streptomycin	Gibco	Cat#15140-122
Trypsin-EDTA (0.05%), phenol red	Gibco	Cat#25200-072
Phosphate-Buffered Saline (PBS), pH 7.4 basic (1X)	Gibco	Cat#C10010500BT
HEPES (1M)	Gibco	Cat#15630-080
Sodium Pyruvate (100 mM)	Gibco	Cat#11360-070
2-Mercaptoethanol	Gibco	Cat#21985-023
L-Glutamine (200 mM)	Gibco	Cat#25030-081
HBSS, calcium, magnesium, no phenol red (1X)	Gibco	Cat#14025092
Seahorse XF Base Medium	Agilent	Cat#102353-100
Recombinant Mouse IL-2 (carrier-free)	Biolegend	Cat#575406
Recombinant Murine TNF-α	PeproTech	Cat#315-01A
Blasticidin	InvivoGen	Cat#ant-bl-05
Puromycin	InvivoGen	Cat#ant-pr-1
SIINFEKL/ OVA Peptide (257-264)	GenScript	Cat#RP10611
Gp100 (25-33), mouse TFA	MCE	Cat#HY-P2506A
BAY-876	MCE	Cat#HY-100017
Phorbol 12-myristate 13-acetate (PMA)	MCE	Cat#HY-18739
Ionomycin MCE Cat#HY-13434	MCE	Cat#HY-13434
Polyethylenimine, Linear (PEI) MW40000	YEASEN	Cat#40816ES02
Opti-MEM	Gibco	Cat#31985070
DAPI	Cell Signaling Technology	Cat#4083S
H2DCFDA	MCE	Cat#HY-D0940
CellTrace CFSE Cell Proliferation Kit, for flow cytometry	Invitrogen	Cat#C34554
CellTrace Violet Cell Proliferation Kit, for flow cytometry	Invitrogen	Cat#C34557
Brefeldin A Solution (1,000X)	Biolegend	Cat#420601
MitoSOX Mitochondrial Superoxide Indicators, for live-cell imaging	Invitrogen	Cat#M36008
TRIzol Reagent	Invitrogen	Cat#15596018
HiScript III 1st Strand cDNA Synthesis Kit (+gDNA wiper)	Vazyme	Cat#R312-01
Taq Pro Universal SYBR qPCR Master Mix	Vazyme	Cat#Q712-02
Dimethyl sulfoxide (DMSO)	Sigma Aldrich	Cat#D2650
Corn oil	MCE	Cat#HY-Y1888
Collagenase type IV	Sigma Aldrich	Cat#C5138

(*Continued on next page*)

Please cite this article in press as: Wu et al., Tumor aerobic glycolysis confers immune evasion through modulating sensitivity to T cell-mediated bystander killing via TNF-α, Cell Metabolism (2023), https://doi.org/10.1016/j.cmet.2023.07.001

Continued

REAGENT or RESOURCE	SOURCE	IDENTIFIER
DNAse type IV	Sigma Aldrich	Cat#D5025
Hyaluronidase type V	Sigma Aldrich	Cat#H6254
Cell Lysis Buffer (10X)	Cell Signaling Technology	Cat#9803S
ACK Lysis Buffer	LEAGENE	Cat#CS0001
Protease inhibitors	Sigma Aldrich	Cat#11873580001
SurePAGE, Bis-Tris, 10x8, 4-12%, 15 wells	GenScript	Cat#M00654
Tris-buffered saline with 0.1% Tween 20 detergent (TBST)	Beyotime	Cat#ST673
Skim Milk powder	BD	Cat#232100
Immobilon Western Chemiluminescent HRP substrate	Millipore	Cat#WBKLS0500
Critical commercial assays		
MojoSort Mouse CD8 T Cell Isolation Kit	Biolegend	Cat#480007
NucleoSpin Blood XL, Maxi kit for DNA from blood	MACHEREY-NAGEL	Cat#740950.50
NucleoSpin Gel and PCR Clean-up	MACHEREY-NAGEL	Cat#740609.250
NucleoSpin Plasmid Transfection-grade	MACHEREY-NAGEL	Cat#740490.250
APC Annexin V Apoptosis Detection Kit with PI	Biolegend	Cat#640932
Intracellular Fixation & Permeabilization Buffer Set	Invitrogen	Cat#88-8824-00
CellTiter-Glo Luminescent Cell Viability Assay	Promega	Cat#G7570
Zombie NIR Fixable Viability Kit	Biolegend	Cat#423106
Pierce BCA Protein Assay Kit	Thermo Scientific	Cat#23225
Deposited data		
Raw and analyzed data	This paper	GEO: GSE215107
Human NSCLC scRNA-seq dataset1	Lambrechts et al.[55]	ArrayExpress: E-MTAB-6149
Human NSCLC scRNA-seq dataset2	Song et al.[56]	GEO: GSE117570
Human NSCLC scRNA-seq dataset3	Zilionis et al.[57]	GEO: GSE127465
Human NSCLC scRNA-seq dataset4	Wang et al.	GEO: GSE143423
Human NSCLC scRNA-seq dataset5	Chi et al.[58]	GEO: GSE150660
Human PAAD scRNA-seq dataset1	Peng et al.[59]	GSA: CRA001160
Human PAAD scRNA-seq dataset2	Moncada et al.[60]	GEO: GSE111672
Human PAAD scRNA-seq dataset3	Schlesinger et al.[61]	GEO: GSE141017
Human PAAD scRNA-seq dataset4	Lin et al.[62]	GEO: GSE154778
Human breast cancer scRNA-seq dataset	Chung et al.[63]	GEO: GSE75688
Experimental models: Cell lines		
Mus musculus: B16F10	National Collection of Authenticated Cell Cultures, Shanghai, China	RRID: CVCL_0159
Mus musculus: LLC	National Collection of Authenticated Cell Cultures, Shanghai, China	RRID: CVCL_4358
Mus musculus: Panc02	Shanghai Biofeng Biotech.	RRID: CVCL_D627
MIA Paca-2	National Collection of Authenticated Cell Cultures, Shanghai, China	RRID: CVCL_0428
Experimental models: Organisms/strains		
Mouse: C57BL/6-Tg(TcraTcrb)1100Mjb/J or OT-I	The Jackson Laboratory	RRID: IMSR_JAX:003831
Mouse: C57BL/6J	Tsinghua University	RRID: IMSR_JAX:000664
Mouse: NOD.Cg-*Prkdc*^{scid} *Il2rg*^{tm1Wjl}/SzJ or NSG	The Jackson Laboratory	RRID: IMSR_JAX:005557

(*Continued on next page*)

Continued

REAGENT or RESOURCE	SOURCE	IDENTIFIER
Mouse: Rag1/Rag2^{tm1Mnz}/Rag1/Rag2^{tm1Mnz}	The Jackson Laboratory	RRID: MGI:3720353
Oligonucleotides		
sgRNA sequences to generate KO cell lines, see Table S2	This paper	N/A
qPCR primer for Cflar-F: GCTCCAGAATGGGCGAAGTAA	This paper	N/A
qPCR primer for Cflar-R: ACGGATGTGCGGAGGTAAAAA	This paper	N/A
qPCR primer for Hprt-F: TCAGTCAACGGGGGACATAAA	This paper	N/A
qPCR primer for Hprt-R: GGGGCTGTACTGCTTAACCAG	This paper	N/A
Recombinant DNA		
LentiCas9-Blast	Addgene	RRID: Addgene_52962
LentiCRISPRv2-Puro	Addgene	RRID: Addgene_52961
LentiCRISPRv2-EGFP	This paper	N/A
psPAX2	Addgene	RRID: Addgene_12260
pMD2.G	Addgene	RRID: Addgene_12259
Mouse sgRNA library Brie in lentiGuide-Puro	Addgene	RRID: Addgene_73633
Software and algorithms		
GraphPad Prism 9	GraphPad	RRID: SCR_002798
FlowJo 10	BD	RRID: SCR_008520
Image-Pro Plus 6.0	Media Cybernetics	RRID: SCR_007369
STAR v2.6.1d	Dobin et al.[64]	RRID: SCR_004463
DESeq2 v1.34.0	Bioconductor	RRID: SCR_000154
MaGeCK	Li et al.[65]	https://sourceforge.net/p/mageck/wiki/Home/

RESOURCE AVAILABILITY

Lead contact

Further information and requests for reagents may be directed to and will be fulfilled by the lead contact, Deng Pan (dpan@tsinghua.edu.cn).

Materials availability

Cell lines generated in this study will be provided by the lead contact under a material transfer agreement.

Data and code availability

- RNA-seq data in this publication have been deposited in the NCBI Gene Expression Omnibus (GEO) (GSE215107). Uncropped western blots and source data can be found in Data S1.
- This paper does not report original code.
- Any additional information required to reanalyze the data reported in this paper is available from the lead contact upon request.

EXPERIMENTAL MODEL AND SUBJECT DETAILS

Cell lines

B16F10 (RRID: CVCL_0159), LLC (RRID: CVCL_4358), and Panc02 (RRID: CVCL_D627) cells were cultured in DMEM supplemented with 10% fetal bovine serum, 100 μg/mL penicillin and 100U/ml streptomycin. MIA Paca-2 (RRID: CVCL_0428) cells were cultured in DMEM supplemented with 10% fetal bovine serum, 2.5% horse serum, 1% Glutamax, 1mM sodium pyruvate, 100 μg/mL penicillin and 100U/ml streptomycin. All cells were cultured at 37 °C in 5% CO_2.

Please cite this article in press as: Wu et al., Tumor aerobic glycolysis confers immune evasion through modulating sensitivity to T cell-mediated bystander killing via TNF-α, Cell Metabolism (2023), https://doi.org/10.1016/j.cmet.2023.07.001

Primary cultures

OT-I CD8+T cells were isolated from mouse spleens using the MojoSort Mouse CD8 T Cell Isolation kit (Biolegend Cat# 480007) and activated using anti-mouse CD3 (Bio X Cell Cat# BE0001-1, RRID: AB_1107634) and anti-mouse CD28 (Bio X Cell Cat# BE0015-1, RRID: AB_1107624) antibodies. CD8 T cells were cultured and expanded in T cell media (RPMI 1640 media with 10% fetal bovine serum, 20mM HEPES, 1mM sodium pyruvate, 0.05mM 2-mercaptoethanol, 2mM L-glutamine and 100U/ml streptomycin, and 100 μg/mL penicillin) with 20ng/ml of recombinant mouse IL-2 (Biolegend Cat#575406). T cells were co-cultured with tumor cells for at least seven days after activation.

Animal studies

Eight to 12-week-old C57BL/6J (RRID: IMSR_JAX:000664) or NSG mice (RRID: IMSR_JAX:005557) female mice were used for all animal experiments. All mice were used in accordance with the guidelines accredited by the Association for Assessment and Accreditation of Laboratory Animal Care International and Institutional Animal Care and Use Committee (IACUC) of Tsinghua University under protocol number 19-PD-1. C57BL/6J and NSG mice were bred at the Laboratory Animal Resources Center of the Tsinghua University. All mice were maintained in pathogen-free facilities.

Human specimens

Human tumor paraffin sections were collected from Zhongnan Hospital of Wuhan University. All samples were obtained from the residual clinical tissue samples after pathological diagnosis. The samples were used with informed consent under a protocol approved by the Medical Ethics Committee of Zhongnan Hospital of Wuhan University. Information about sex, age, and tumor stages is summarized in Table S1.

METHOD DETAILS

CRISPR screens

Genome-wide tumor-CTL co-culture screen in LLC and Panc02 cells

Panc02-Cas9 and LLC-Cas9 were generated by transfection with lentivirus encoding Cas9-Blast (RRID: Addgene_52962) and selected with 10μg/mL blasticidin (InvivoGen Catalog# ant-bl-05) for 10 days. Screening was performed as described previously.[19] LLC-Cas9 and Panc02-Cas9 were transfected into the Brie lentivirus library (Addgene # 73633) at an infection rate around 10%. After 36 hours of transfection, cells that had been transduced were selected using 2 μg/ml of puromycin (InvivoGen Cat#ant-pr-1) for 4 days. Following 10 days of viral transfection, the cells were assigned into an experimental group and a control group, with three replicates for each group. Each replicate contained 8×10^7 cells (~1000x in sgRNA coverage). The experimental groups were exposed to 100 ng/ml of SIINFEKL peptide for 2 hours prior to the addition of activated OT-1 CD8+ T cells, while the control group did not receive the peptide. Both the experimental and control groups were co-cultured with activated OT-1 CD8+ T cells for 24 hours at 1:1 E:T ratio. Following a 24-hour co-culture period, T cells were removed by discarding the supernatant, after which the tumor cells were washed twice with PBS and allowed to recover for an additional 24 hours. The tumor cells were harvested using trypsin and the genomic DNA was extracted from the cells using the NucleoSpin Blood XL kit (MACHEREY-NAGEL Cat# 740950.50), following the manufacturer's instructions. Amplification of the sgRNA cassettes by PCR was performed according to the broad GPP protocol. https://portals.broadinstitute.org/gpp/public/resources/protocols

Genome-wide CRISPR rescue screen after treatment with BAY-876 and CTL-derived conditioned media

The same LLC-Cas9 cells transduced with Brie library as described in (a) were divided into four conditions: (1) left untreated, (2) pretreated with BAY-876 (MCE Catalog# HY-100017, 200nM) for 24 h, (3) treated with 25 mL T cell-derived conditioned media for 48 hours in a 15 cm dish and (4) pretreated with BAY-876 (200nM) for 48 h and then treated with T cell-derived conditioned media for another 48 h. There were two replicates for conditions (1) and (2) and three replicates for conditions (3) and (4). Each replicate contained 8×10^7 cells per well. Under all conditions, the cells were collected for DNA extraction at the same time. T cell-derived conditioned media were collected and filtered from OT-I CTL and LLC co-culture at a 1:1 ET ratio for 24h.

Data analysis for CRISPR screens

MaGeCK was used to process and analyze the CRISPR screen data.[65] Fastq reads from the CRISPR screen were processed using the count module. The RRA module (default setting) was used to calculate $\log_2$ fold changes and p-values of the genes. Custom R (v4.1.3) scripts were used to visualize the data.

Generation of KO cell lines

The sgRNA sequences were used to generate KO cell lines were listed in Table S2. For Glut1, Gpi1 sgRNA was cloned into LentiCRISPRv2-Puro (RRID: Addgene_52961) and confirmed using Sanger sequencing. sgRNA constructs were co-transfected with psPAX2 (RRID: Addgene_12260) and pMD2.G (RRID: Addgene_12259) mixed with 1:4 PEI in Opti-MEM for lentivirus production. The virus was harvested 48 h after transfection and used to infect the LLC and Panc02 cells. Puromycin (2 ng/mL) was added to the culture for selection of KO cell lines.

To generate TNF receptor-KO cell lines, sgRNA against *Tnfrsf1a* was cloned into LentiCRISPRv2-EGFP, a construct generated in-house by replacing the puromycin resistance protein with EGFP. LLC cells were infected with lentiviruses expressing sgRNA

targeting *Tnfrsf1a* and control sgRNAs. Five days post-infection, the cells were stained with PE anti-mouse CD120a antibody (BioLegend Cat#113004 RRID: AB_313533). Control (GFP+) and TNFR KO (GFP+ TNFR-) cells were sorted. Control and *Tnfrsf1a*-KO cells were then transfected with lentiviruses expressing Glut1 and Gpi1 sgRNAs, respectively.

In vitro tumor-CTL co-culture and cytokine treatment experiments

Glut1 or Gpi1 KO cells (GFP-negative) were mixed with control cells (GFP-positive) at a 1:1 ratio and then maintained for at least two passages. These cells were used for the *in vitro* competition experiments, as described below.

Tumor-CTL co-culture experiments

0.6×10^6 tumor cells in a 6-well plate were either pulsed or unpulsed with 100 ng/ml SIINFEKL peptide (GenScript #RP10611) for 2 h in an incubator. After pulsing, the mixed cells were co-cultured with *in vitro*-activated OT-I CD8+ T cells at the indicated effector-to-target ratios in a 6-well plate. After 24 h of co-culture, T cells were removed and the tumor was recovered for another 24 h. Cells were collected and stained with 0.1μg/mL CD45-APC (Biolegend Cat #157606 RRID: AB_2876537), 1μg/mL DAPI (Cell Signaling Technology Cat# 4083S) in 50μL FACS buffer for 20 min at room temperature, resuspend in 200μl FACS buffer, and analyzed by FACS (CytoFLEX S, Beckman). Fold-changes in the percentage of mutant tumor cells in the mixture in the presence or absence of T cells were determined.

Co-culture experiments using transwell

In a 6-well plate, 0.6×10^6 mixture tumor cells were seeded in the lower well and 0.4×10^6 mixture tumor cells were seeded in the upper well of the 0.4 μm transwell (Corning Cat# 3450), respectively. Cells in the upper well were treated with 100 ng/ml SIINFEKL peptide or 1μg/ml of gp100 peptide for 2 h in an incubator. After pulsing, the mixed cells in the upper well were co-cultured with activated OT-I CD8+ T cells at an E:T ratio of 1:4. After 24 h of co-culture, T cells were removed and the tumor was recovered for another 24 h. Cells in the upper and lower wells were stained with CD45-APC and DAPI for FACS analysis, as described above.

TNFa blocking experiment

To perform the TNFα blocking experiment, 0.3×10^6 tumor cells were plated in a 12-well plate and pulsed with 100 ng/ml SIINFEKL for 2 hours. For the control group, tumor cells were cultured with T cell medium without the addition of OT-I T cells. In the killing group, 0.1×10^6 OT-I T cells were added to 1 ml of T cell medium with or without 200 μg/ml TNFα blocking antibodies (BioXcell Cat# BE0058). After 24 hours of co-culture, the cells were harvested and stained with CD45-APC and DAPI. Live tumor cell numbers were then counted by FACS. The fraction of viable cells was calculated using the following equation: Fraction of viable cells = (number of live tumor cells in killing group) / (number of live tumor cells in control group).

In vitro CTL experiments to determine Glut1 inhibition effects on T cell functions

T cell activation and proliferation experiments

Naive CD8 T cells were isolated from C57BL/6J mouse (RRID: IMSR_JAX:000664) spleens using the MojoSort Mouse CD8 T Cell Isolation kit (Biolegend Cat# 480007). After washing once with PBS, T cells were stained with 5 μM CellTrace Violet in PBS for 15 minutes at room temperature. 0.6×10^6 naive T cells were used for FACS to check the baseline expression levels of T cell activation markers and the rest naive T cells were activated and expanded as described above. T cells were either treated or untreated with BAY-876 (200nM) and then harvested for flow cytometry analysis until day4. Cells were first stained with Zombie-NIR Fixable Viability Kit (BioLegend Cat# 423106) in PBS, and then stained with anti-mouse-CD8 (Biolegend Cat# 100707, RRID: AB_312746) and anti-mouse CD69 Antibody (Biolegend Cat# 104531, RRID: AB_2562326). Beckman Coulter CytoFLEX S was used for data collection and FlowJo (RRID: SCR_008520) was used for data analysis.

T cell cytokine production experiments

Naive OT-I T cells were isolated from OT-I transgenic mouse (RRID: IMSR_JAX:003831) spleens using the MojoSort Mouse CD8 T Cell Isolation kit (Biolegend Cat# 480007). OT-I T cells were activated and expanded as described above. T cells were co-cultured with tumor cells for cytokine production assay at or after day7 following activation. 24 hours before co-culture, OT-I T cells were either treated or untreated with BAY-876 (200nM). 0.2×10^6 tumor cells in a 12-well plate were pulsed with 100 ng/mL SIINFEKL peptide (GenScript #RP10611) for 2 hours in an incubator. After pulsing, tumor cells were co-cultured with *in vitro*-activated OT-I CD8+ T cells in the presence of 5 μg/mL Brefeldin A (BFA, Biolegend Cat#420601) at the indicated effector-to-target ratios in a 12-well plate. As positive controls, T cells were treated with 20 ng/mL Phorbol 12-myristate 13-acetate (PMA, MCE Cat#HY-18739) and 2 μg/mL ionomycin (MCE Cat#HY-13434) in the presence of BFA. After 6 hours of co-culture, T cells were harvested for flow cytometry analysis. Cells were first stained with Zombie-NIR Fixable Viability Kit (BioLegend Cat# 423106) and anti-mouse-CD8 (Biolegend Cat#100707, RRID: AB_312746) in PBS for 15 min at room temperature. For intracellular cytokine staining, cells were fixed and permeabilized with an intracellular fixation and permeabilization buffer set (Invitrogen Cat# 88-8824-00), then stained with anti-mouse IFNγ (Biolegend Cat#505809, RRID: AB_315403) and anti-mouse TNFα (Biolegend Cat#506303, RRID: AB_315424) in permeabilization buffer (Invitrogen Cat#00-8333-56) for 30 min at room temperature. Beckman Coulter CytoFLEX S was used for data collection and FlowJo (RRID: SCR_008520) was used for data analysis.

T cell target killing experiments

Naive OT-I T cells were isolated from OT-I transgenic mouse (RRID: IMSR_JAX:003831) spleens using the MojoSort Mouse CD8 T Cell Isolation kit (Biolegend Cat# 480007). OT-I T cells were activated and expanded as described above. 0.6×10^6 LLC cells in a 6-well plate were either pulsed or unpulsed with 100 ng/ml SIINFEKL peptide (GenScript #RP10611) for 2 h in an incubator. After pulsing, tumor cells were co-cultured with *in vitro*-activated OT-I CD8+ T cells at the indicated effector-to-target ratios in a 6-well

Please cite this article in press as: Wu et al., Tumor aerobic glycolysis confers immune evasion through modulating sensitivity to T cell-mediated bystander killing via TNF-α, Cell Metabolism (2023), https://doi.org/10.1016/j.cmet.2023.07.001

plate. After 12 h of co-culture, T cells were removed and tumor cells were harvested and stained with 0.1μg/mL CD45-APC (Biolegend Cat #157606 RRID: AB_2876537), 1μg/mL DAPI (Cell Signaling Technology Cat# 4083S) in 50μL FACS buffer for 20 min at room temperature, resuspend in 200μl FACS buffer, and analyzed by FACS (CytoFLEX S, Beckman).

In vitro FACS experiments to determine cell apoptosis and ROS level

Cell apoptosis staining experiments

Tumor cells (0.5×10^6) were plated in 6-well plates per well and incubated for 48 h with complete medium containing TNFα, BAY-876, or both. For cell apoptosis staining, cells were stained with APC Annexin V Apoptosis Detection Kit with PI (BioLegend Cat# 640932) following the manufacturer's protocol. For cleaved Caspase-8 staining, the cells were fixed and permeabilized with an intracellular fixation and permeabilization buffer set (eBiosciences Cat# 88-8824-00) for intracellular staining of cleaved Caspase-8 (Cell Signaling Technology Cat# 8592, RRID: AB_10891784) primary antibody. The cells were then stained with anti-rabbit IgG antibody (Cell Signaling Technology Cat# 4412, RRID: AB_1904025) and analyzed using flow cytometry.

ROS staining experiments

Cells were harvested with 0.05% trypsin-EDTA solution, incubated with 5 μM H2DCFDA (MCE Cat#HY-D0940) solution in PBS in the dark for 30 min at 37°C, suspended in FACS buffer, and immediately analyzed by flow cytometry. Mitochondrial ROS levels were measured using MitoSOX Red (Invitrogen Cat#M36008) according to the manufacturer's protocol and analyzed using a flow cytometer.

Real time qPCR experiments

Total RNA was purified using TRIzol reagent (Invitrogen, Cat# 15596018) according to the manufacturer's protocol. Extracted RNA (1 μg) was transcribed into cDNA using the HiScript III 1st Strand cDNA Synthesis Kit (Vazyme Cat# R312-01), according to the manufacturer's protocol. cDNA samples were diluted and used for realtime qPCR (RT-qPCR). Taq pro universal SYBR qPCR master mix (Vazyme Cat# Q712-02) and gene-specific primers were used for PCR amplification and detection on a LightCycler480 (Roche). RT-qPCR data were normalized to Hprt mRNA. The following primers (5'-3') were used: Cflar-F: GCTCCAGAATGGGCGAAGTAA, Cflar-R: ACGGATGTGCGGAGGTAAAAA Hprt-F: TCAGTCAACGGGGGACATAAA, Hprt-R: GGGGCTGTACTGCTTAACCAG

Cell titer Glo experiments

For cell growth and viability experiments, 20,000 cells were plated in 96-well plates and live cells were quantified using Cell Titer-Glo (Promega Cat# G7570). Viability experiments were repeated for confirmation as follows: 0.2×10^6 cells were plated in 12-well plates and treated with the indicated cytokines. The cells were stained with DAPI and resuspended in the FACS buffer. Live cells were counted using CytoFLEX S (Beckman).

Seahorse experiments

Tumor cells were seeded onto 96-well plates (Seahorse XFe96 FluxPak, Agilent Cat#102416-100) at 10,000 per well for Panc02 cells and 12,000 per well for LLC cells overnight. The OCR and ECAR measurements were performed using a Seahorse XFe96 analyzer (Seahorse Biosciences). Cells were cultured in DMEM's medium (Agilent Cat# 102353-100, adjusted to PH7.4) supplemented with 4.5 g/L glucose (Gibco) and 2 mM glutamine (Gibco). The OCR and ECAR were measured in response to sequential injections of oligomycin (1 mM), FCCP (1 mM), and antimycin/rotenone (1 mM). For glycolysis stress test, The ECAR were measured in response to sequential injections of glucose (10 mM), oligomycin (1 μM), oligomycin (2-DG, 1 μM). Proton Efflux Rate (PER) were calculated by Agilent Seahorse Wave Desktop using following equation: PER (pmol H+/min) = ECAR (mpH/min) × Buffer Factor (mmol/L/pH) × Geometric Volume (μL) × Kvol.

Mouse tumor experiments

For tumor challenges, 1×10^6 LLC, 1×10^6 B16F10 or 2×10^6 Panc02 cells were resuspended in HBSS and injected subcutaneously (s.c.) into the flanks of mice. For anti-PD-1 treatment, mice bearing tumors were intraperitoneally (i.p.) injected with 200 μg of anti-PD1 antibodies (Bio X Cell Cat# BE0273, RRID: AB_2687796) on days 9 and 12 for LLC and on days 4, 7, and 10 for B16F10. For BAY-876 treatment, 80 μg BAY-876 or the same volume of vehicle (10%DMSO and 90% corn oil) was injected intratumorally (i.t.) on days 4, 7, 10, and 13. The length and width were measured every 3-4 days when the tumors became palpable, and tumor volume was calculated using the formula: (length × width^2)/2. The endpoint was recorded when the tumor diameter reached 2.0 cm or mice died. Randomization was performed on age and sex-matched mice when possible. When measuring the tumor size, investigators were blinded for sample allocations when feasible.

In vivo competition experiments

Two types of cell mixtures were generated for *in vivo* competition experiments. Control mixture cells were mixed at a 1:1 ratio of two control LLC cells that expressed EGFP and tdTomato. Glut1 KO mixture cells were constituted of control cells (EGFP) and Glut1 KO cells (tdTomato) at an approximately 1:1 ratio. These mixed cells were then transplanted into mice with different levels of selection pressure, including NSG mice, wild-type B6 mice, and B6 mice treated with 200 μg anti-PD-1. On day 14-16, tumors were harvested and analyzed by flow cytometry to determine the EGFP:tdTomato ratio.

Analysis of tumor infiltrating lymphocytes

Tumors were dissociated in GentleMACS dissociator with 1 mg/ml collagenase type IV, 20 units/ml DNAse type IV and 0.1mg/ml hyaluronidase type V for 30 min at 37 °C. Cells were passed through a 70-μm filter and a small fraction was used for FACS. The following antibodies were used: anti-mouse-CD45 (BioLegend Cat#103133, RRID: AB_10899570), anti-mouse-CD3 (BioLegend Cat#100204, RRID: AB_312661), anti-mouse-CD8a (BioLegend Cat# 100708, RRID: AB_312747), anti-mouse-CD4 (BioLegend Cat#100559, RRID: AB_2562608), anti-mouse-NK1.1 (eBioscience Cat#17-5941-81, RRID: AB_469478), and anti-Granzyme B-PE/CY7 (BioLegend Cat#372214, RRID: AB_2728381). Cells were first stained with Zombie-NIR Fixable Viability Kit (BioLegend Cat# 423106) in PBS, and then stained with anti-mouse CD16/32 (BioLegend Cat#101320, RRID: AB_1574975) to block the IgG Fc receptor. The cells were stained with surface markers, fixed, and permeabilized for intracellular staining. Beckman Coulter CytoFLEX S was used for data collection and FlowJo (RRID: SCR_008520) was used for data analysis.

Adoptive transfer experiments

10^6 of LLC-OVA-NGFR cells were subcutaneously injected to 8-week-old female Rag1 KO mice. On day 9, $2x10^6$ activated OT-I T cells were transferred by tail vein injection. On day 16, tumors were harvested and dissociated as described in the above section. 10^6 live tumor cells (gated on NGFR+) and OT-I T cells (gated on CD45+ and CD8+) were sorted and subjected to RNAseq.

Western blot

Whole-cell lysates were solubilized in cell lysis buffer (Cell Signaling Technology Cat# 9803) with protease inhibitors (Sigma-Aldrich) and clarified using sonicator at 25% amplitude using 5 sec pulses. Protein concentrations were assayed using BCA Protein Assay (Thermo Fisher Cat# 23225) and 20 μg total protein was loaded per lane onto 4-12% gradient, SurePAGE, Bis-Tris gels (GenScript Cat# M00654). Gels were transferred to Immobilon PVDF membranes (Millipore). Membranes were blocked in TBST containing 5% nonfat milk for 1 h at room temperature and were overnight incubated with indicated antibodies followed by incubating with anti-rabbit HRP (Cell Signaling Technology Cat# 7074, RRID: AB_2099233). Blots were incubated in Immobilon Western HRP substrate (Millipore). Chemiluminescence was captured using Amersham Imager 600 (GE).

Immunofluorescence staining of human samples

Paraffin blocks were cut into 3–5 mm sections and adhered to glass slides. The slides were stained with anti-Glut1 (Abcam Cat# ab115730, RRID: AB_10903230), anti-Ki67 (Abcam Cat# ab15580, RRID: AB_443209), and anti-CD45 (Servicebio, Cat# GB113885, 1:500 dilution) using Tyramide Signal Amplification (TSA) technology. The slides were then incubated with DAPI and washed with PBS. Slides were scanned using a Pannoramic MIDI (3DHISTECH) automatic digital slide scanner, visualized using CaseViewer2.4 and analyzed using Image-Pro Plus 6.0 (RRID: SCR_007369).

Bulk RNA-seq

LLC cells were either pretreated or left untreated for 200nM BAY-876 for 24 hours, followed by treatment with 20ng/ml TNFα or left untreated for 32 hours. The cells were washed with PBS and lysed using TRIzol (Invitrogen, Cat# 15596026). The reads were aligned to the mouse reference genome mm10 using STAR[64] (RRID: SCR_004463). Feature count was used to map aligned reads to genes and generate a gene count matrix. Statistical analysis of the differentially expressed genes was performed using the DESeq2 R package (RRID: SCR_000154).

Single cell RNA-seq analysis

SingleCellExperiment (v1.16.0) was used for quality control purposes. Cells with low log-transformed library size, low log-transformed number of expressed genes, or high mitochondrial proportions that were more than 3 MADs (median absolute deviation) from the median were identified as low-quality cells and discarded. Seurat (v4.1.1) was used for integration,[66] normalization, dimensionality reduction, clustering, UMAP visualization, and marker gene detection, based on which manual annotation was performed for each cluster. Other downstream analyses were performed using custom R (v4.1.3) scripts.

Single cell analysis for human samples

Human scRNA-seq datasets[55–63] (see Table S3) were obtained from public databases. All datasets were pre-processed using the Seurat standard pre-processing workflow (https://satijalab.org/seurat/articles/pbmc3k_tutorial.html), and clusters of each dataset were annotated according to the marker genes. In each cell type in each dataset, the frequencies of cells expressing SLC2A1 or SLC2A3 were calculated.

Analysis of ICB cohorts

Human ICB datasets[40,67–78] (see Table S4) are obtained from public databases. Samples were stratified by response status, and the HALLMARK_GLYCOLYSIS signature levels were compared between the responders and non-responders. In our study, samples were separated into immune-cold and -hot samples, which were defined by CTL level that was calculated by the average expression of CD8A, CD8B, GZMA, GZMB, and PRF1.

Please cite this article in press as: Wu et al., Tumor aerobic glycolysis confers immune evasion through modulating sensitivity to T cell-mediated bystander killing via TNF-α, Cell Metabolism (2023), https://doi.org/10.1016/j.cmet.2023.07.001

Analysis of TCGA cohorts

Transcriptome data and clinical data were obtained from the TCGA Data Portal (https://www.cancer.gov/tcga). We chose all 33 cancer types with transcriptome data available for cancer samples. Only those samples in the clinical category of "primary tumor" were used for this study.

QUANTIFICATION AND STATISTICAL ANALYSIS

Statistical analyses were performed by using GraphPad Prism 9 software (RRID:SCR_002798). Unpaired student's t-test, 1-way ANOVA or 2-way ANOVA test were used as indicated (ns: not significant, *: $p<0.05$, **: $p<0.01$, ***: $p<0.001$, ****: $p<0.0001$). For power analysis, group sizes for *in vivo* experiments were determined empirically based upon prior experience of the corresponding tumor models. Similarly, group sizes *in vitro* were selected based on our prior knowledge of the variation on the experiments.

For ICB analysis (Figures 7B and 7C), P values are derived from linear regression model which uses HALLMARK_GLYCOLYSIS expression level to predict responding status (responder vs. non-responder). For TCGA analysis (Figures 7D and 7E), p values are derived from log-rank test that compares the survival distributions of the $Glycolysis^{low}$/ TNF^{high} group and the $Glycolysis^{high}$/ TNF^{low} group (D) or the survival distributions of the $GLUT1^{low}$/ TNF^{high} group and the $GLUT1^{high}$/ TNF^{low} group (E).

Cell Metabolism, Volume *35*

Supplemental information

Tumor aerobic glycolysis confers immune evasion through modulating sensitivity to T cell-mediated bystander killing via TNF-α

Lijian Wu, Yiteng Jin, Xi Zhao, Kaiyang Tang, Yaoning Zhao, Linjie Tong, Xuerong Yu, Ke Xiong, Ce Luo, Jiajun Zhu, Fubing Wang, Zexian Zeng, and Deng Pan

Supplementary Figures and Tables

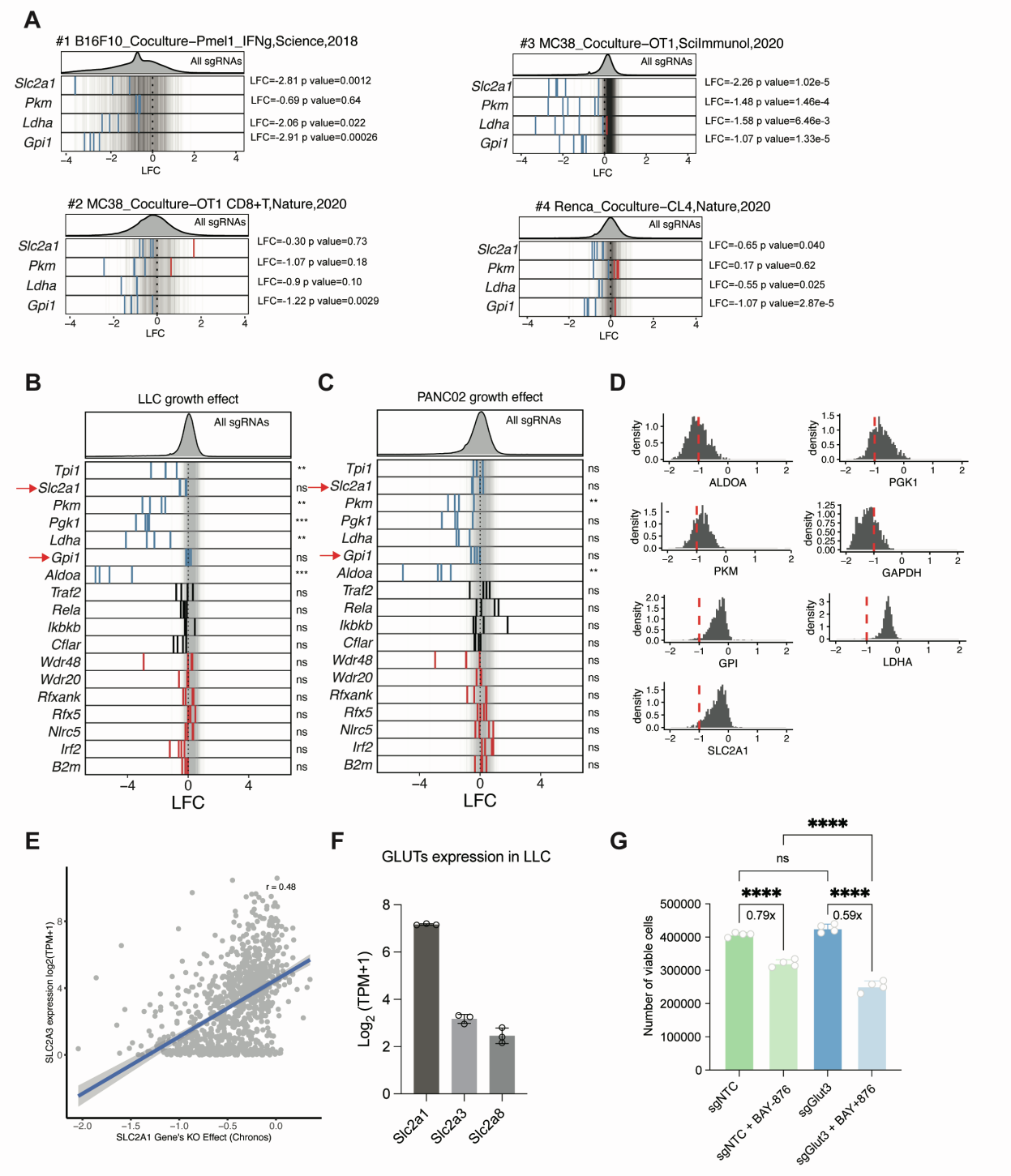

Figure S1. Genome-wide CRISPR screens identified glycolysis genes Glut1 and Gpi1 are required for resistance to T cell-mediated killing, Related to Figure 1.

(**A)** Re-analysis of published CRISPR screens by MAGeCK. Log_2 fold change of sgRNAs' effect on tumor's sensitivity to T cell-mediated killing. Dark grey lines represent control sgRNAs. Blue and red lines represent depleted and enriched sgRNAs upon co-culture with T cells, respectively.

(**B-C**) Log2 fold change of sgRNAs' effect on cell proliferation were plotted in LLC and Panc2 screens, respectively.

(**D**) Essentiality of glycolysis genes in CCLE screen data. A panel of glycolysis gene's KO effect on cell proliferation in CCLE cell lines from DepMap portal. A lower Chronos score indicates higher essentiality of a given gene. Red dashed line marks the Chronos score -1, which is normally considered as the median Chronos score for pan-essential genes.

(**E**) Scatter plot of the essentiality score of GLUT1 (x-axis) and the expression of GLUT3 (SLC2A3). Each dot represents a cell line in CCLE database. Pearson's correlation co-efficient is indicated.

(**F**) The expression level Log2 (TPM+1) of indicated glucose transporters in LLC cells according to RNA-seq data generated in this study (n = 3).

(**G**) Control and Glut3 KO LLC cells were treated with 200nM BAY-876 for 48 hours, respectively (n = 4). The number of viable cells were quantified by DAPI staining using FACS. Data are represented as means ± SD in (F-G). **P < 0.01, ***P < 0.001 and ****P < 0.0001 by one-way ANOVA (G). n.s., not significant.

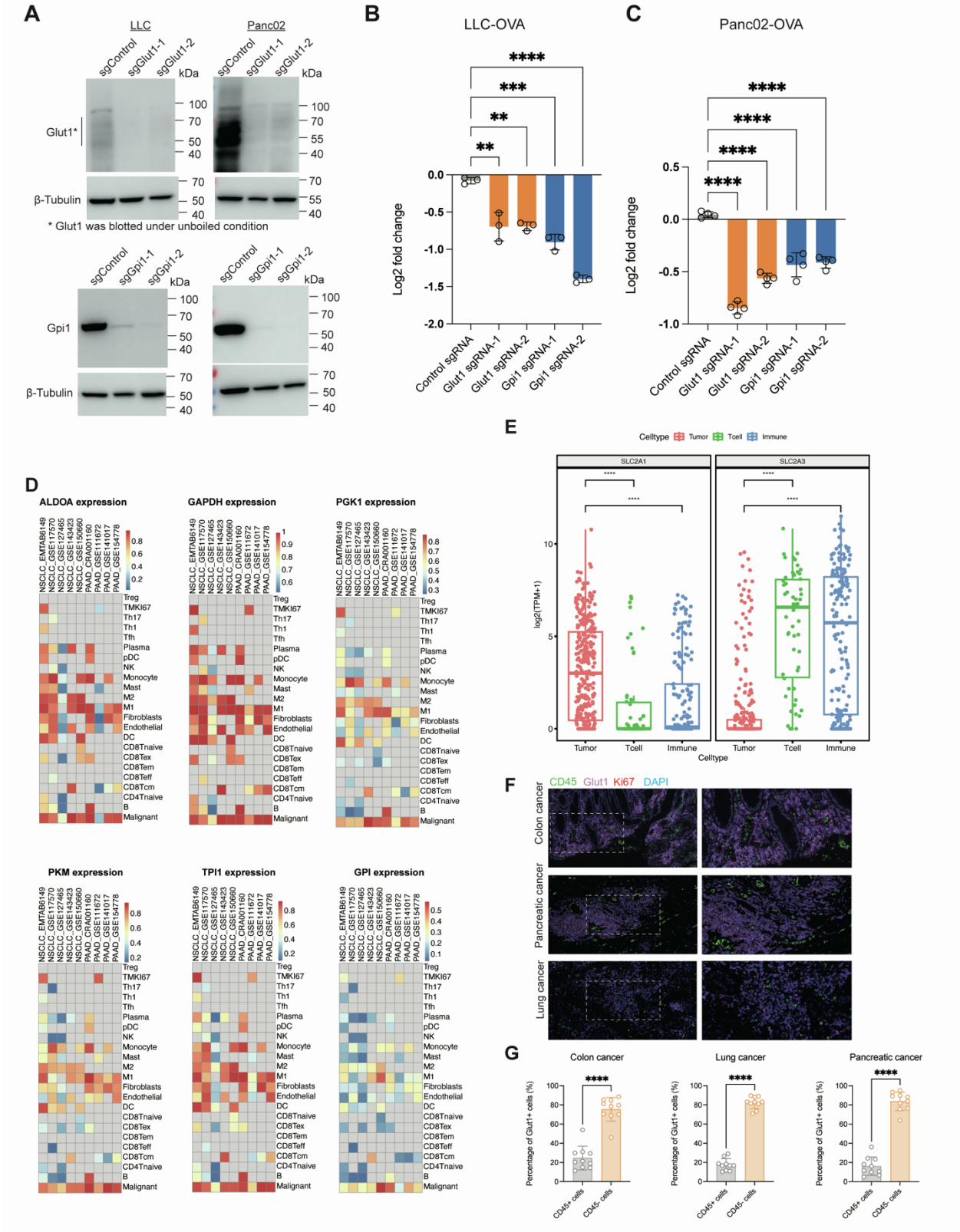
A
LLC
Panc02
sgControl
sgGlut1-1
sgGlut1-2
kDa
Glut1*
β-Tubulin
* Glut1 was blotted under unboiled condition
sgGpi1-1
sgGpi1-2
Gpi1
B
LLC-OVA
Log2 fold change
Control sgRNA
Glut1 sgRNA-1
Glut1 sgRNA-2
Gpi1 sgRNA-1
Gpi1 sgRNA-2
C
Panc02-OVA
D
ALDOA expression
GAPDH expression
PGK1 expression
PKM expression
TPI1 expression
GPI expression
Treg
TMKI67
Th17
Th1
Tfh
Plasma
pDC
NK
Monocyte
Mast
M2
M1
Fibroblasts
Endothelial
DC
CD8Tnaive
CD8Tex
CD8Tem
CD8Teff
CD8Tcm
CD4Tnaive
B
Malignant
E
Celltype Tumor Tcell Immune
SLC2A1
SLC2A3
log2(TPM+1)
F
CD45 Glut1 Ki67 DAPI
Colon cancer
Pancreatic cancer
Lung cancer
G
Colon cancer
Lung cancer
Pancreatic cancer
Percentage of Glut1+ cells (%)
CD45+ cells
CD45- cells

Figure S2. The differential expression pattern of Glut1 and Glut3 in tumor and immune cells, Related to Figure 1.

(**A**) Western blot analysis of Glut1 and Gpi1 protein level in indicated cells.

(**B-C**) *In vitro* competition assay based on tumor-CTL co-culture. GFP labelled LLC-OVA (B, n = 3) or Panc02-OVA (C, n = 4) cells were mixed with GFP- cells transduced with sgRNA targeting control DNA, Glut1 or Gpi1, respectively. These cell mixtures were then co-cultured with pre-activated OT-I T cells. Log2 fold change of the percentage KO cells upon co-culture with OT-I T cells were shown.

(**D**) Heatmaps of expression frequency of a panel of glycolysis genes in indicated cell types in NSCLC and PAAD cancer cohorts.

(**E**) The expression levels of GLUT1 (SLC2A1) and GLUT3 (SLC2A3) in tumor and immune cells respectively, were shown in a Smart-Seq scRNAseq cohort (GSE75688).

(**F**) Representative multi-color immunofluorescence (IF) staining of from an NSCLC sample. The staining images indicate CD45 (green), Ki67 (red), Glut1 (pink), and DAPI (blue).

(**G**) Quantification of percentage of GLUT1+ cells in CD45+ and CD45- cells from IF staining images of NSCLC, PAAD and COAD (n = 10 for each cancer type).

Data are represented as means ± SD. **P < 0.01, ***P < 0.001 and ****P < 0.0001 by one-way ANOVA in (B-C) and unpaired Student's t test in (G).

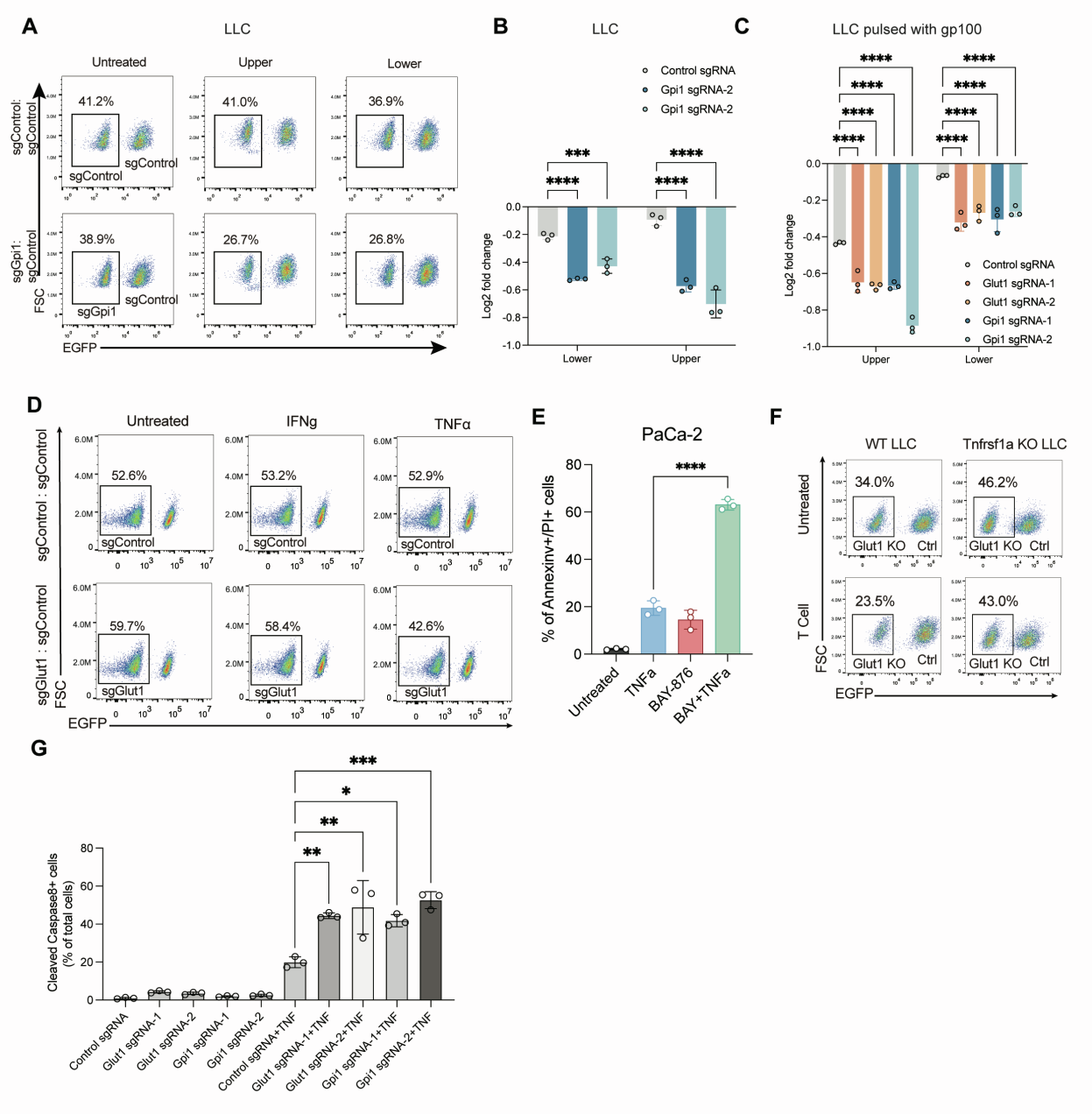

Figure S3. Inactivation of Glut1 sensitized tumor cells to indirect killing mediated by CTLs, Related to Figure 2-3.

(**A**) Representative FACS results showing the percentage of Gpi1 KO cells (GFP-) in the upper and lower wells, respectively.

(**B**) Summary of log2 fold change of the percentage of Gpi1 KO cells as compared with control upon co-culture with OT-I T cells in the transwell experiment (n = 3).

(**C**) LLC cells were pulsed with gp100 peptide prior to addition of Pmel-1 T cells in the upper well. Summary of log2 fold change of the percentage of LLC cells as compared with control upon co-culture with Pmel-1 T cells in the transwell experiment (n = 3).

(**D**) Representative FACS results showing the percentage of Glut1 KO cells (GFP-) upon treatment with indicated cytokines

(**E**) Annexin V and PI staining in MIA PaCa-2 cells pretreated with BAY-876 (200nM) for 24 hours, followed by treatment with TNFα (40ng/ml) or left untreated for 48 hours (n = 3).

(**F**) Representative FACS data for Figure 3F. The FACS plots show the ratio change of Glut1 KO in control and Tnfrsf1a KO LLC cells upon adding OT-I T cells.

(**G**) Control, Glut1 KO and Gpi1 KO LLC cells were either untreated or treated with 20ng/ml TNFα for 48 hours. Cleaved Caspase 8 was determined by FACS (n = 3).

For panel B,C,E,G, data are representative of means $\pm$ SD and p values were determined by one-way ANOVA.

Data are represented as means $\pm$ SD in (B, C, E, G). *P < 0.05, **P < 0.01, ***P < 0.001 and ****P < 0.0001 by two-way ANOVA in (B-C) and one-way ANOVA (E, G).

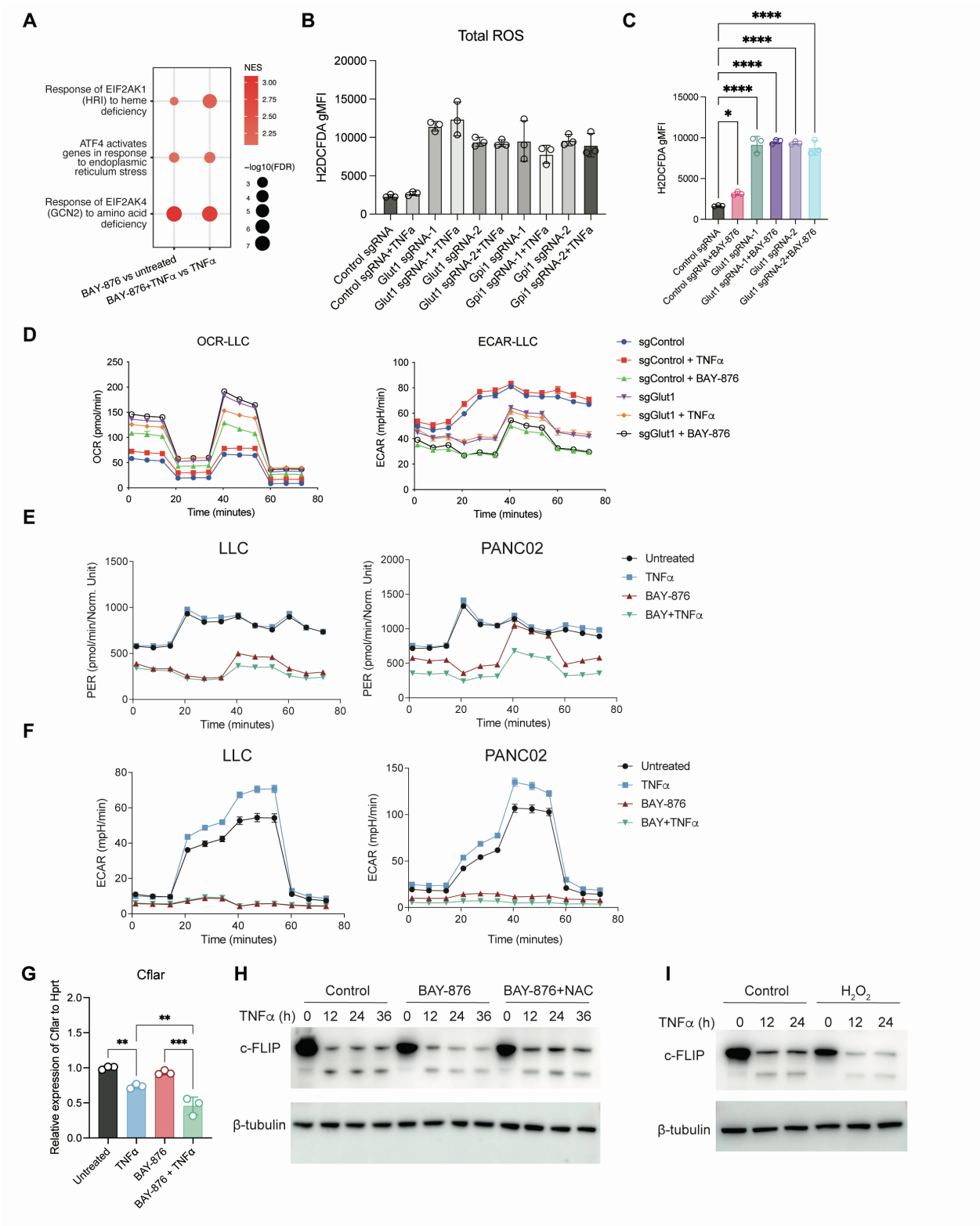

Figure S4. Glut1 inhibition elevates OXPHOS and ROS production, Related to Figure 4.

(**A**) Pre-ranked Gene set enrichment analysis of differential expressed genes in two comparisons: (1) BAY-876 vs untreated, and (2) BAY-876 + TNFα treated vs. TNFα treated LLC cells. ATF4 related gene sets are highlighted.

(**B**) Control, Glut1 KO and Gpi1 KO LLC cells were either untreated or treated with 20ng/ml TNFα for 48 hours. H2-DCFDA staining is determined by FACS (n = 3).

(**C**) Control and Glut1 KO cells were treated with 200nM BAY-876 for 48 hours and the level of H2-DCFDA staining is shown (n = 3).

(**D**) Control and Glut1 KO LLC cells were either pretreated or left untreated with BAY-876 (200nM) for 24 hours, followed by treatment with TNFα (20 ng/ml) or left untreated for 24 hours. Seahorse experiments were used to determine OCR and ECAR.

(**E**) PER is analyzed for the experiments presented in Figure 4E-F.

(**F**) Glycolysis stress test was performed for the cells with same treatment condition as in Figure 4E-F.

(**G**) LLC cells were either pretreated or left untreated for 200nM BAY-876 for 24 hours, followed by treatment with 20ng/ml TNFα or left untreated for 32 hours. qPCR analysis of the relative expression level of *Cflar* to *Hprt* as a housekeeping gene (n = 3 technical replicates from 3 biological replicates for each group).

(**H**) LLC cells were either pretreated with 200nM BAY-876 or 200nM BAY-876 and 1mM NAC for 24 hours, respectively, followed by treatment with 20ng/ml TNFα for indicated time points. WB analysis of c-FLIP levels were shown.

(**I**) LLC cells were treated with 300μM of H_2O_2 for 12 hours, followed by treatment with 20ng/ml TNFα for indicated time points. WB analysis of c-FLIP levels were shown.

Data are represented as means ± SD in (B, C, G) and means ± SEM in (D, E, F). *P < 0.05, **P < 0.01, ***P < 0.001 and ****P < 0.0001 by one-way ANOVA in (C, G).

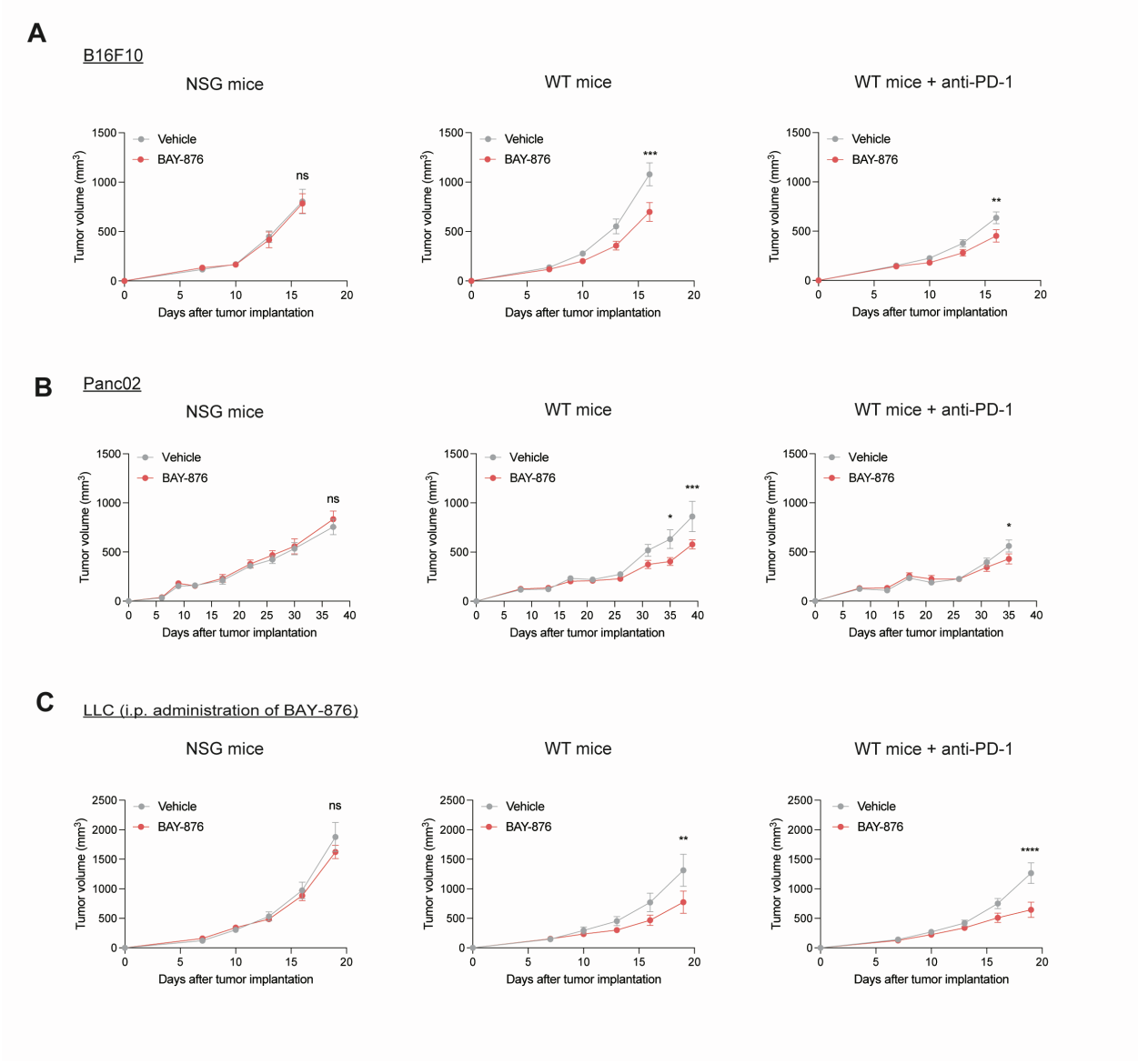

Figure S5. Inactivation of Glut1 sensitized tumors to anti-tumor immunity in mouse models, Related to Figure 6.

(**A-C**) Tumor volume following intratumoral (**A**-**B**), or intraperitoneal (**C**) administration of vehicle control (10% DMSO and 90% corn oil) or Glut1 inhibitor BAY-876 in NSG, wild-type (WT) C57BL/6 mice and WT mice treated with anti-PD-1 in B16F10 (**A**), Panc02 models (**B**) and LLC (**C**) models. n = 6-10 mice per group. For all panels, data are data are representative of means ± SEM and p values were determined by two-way ANOVA.

Data are represented as means ± SEM. *P < 0.05, **P < 0.01, ***P < 0.001 and ****P < 0.0001 by two-way ANOVA. n.s., not significant.

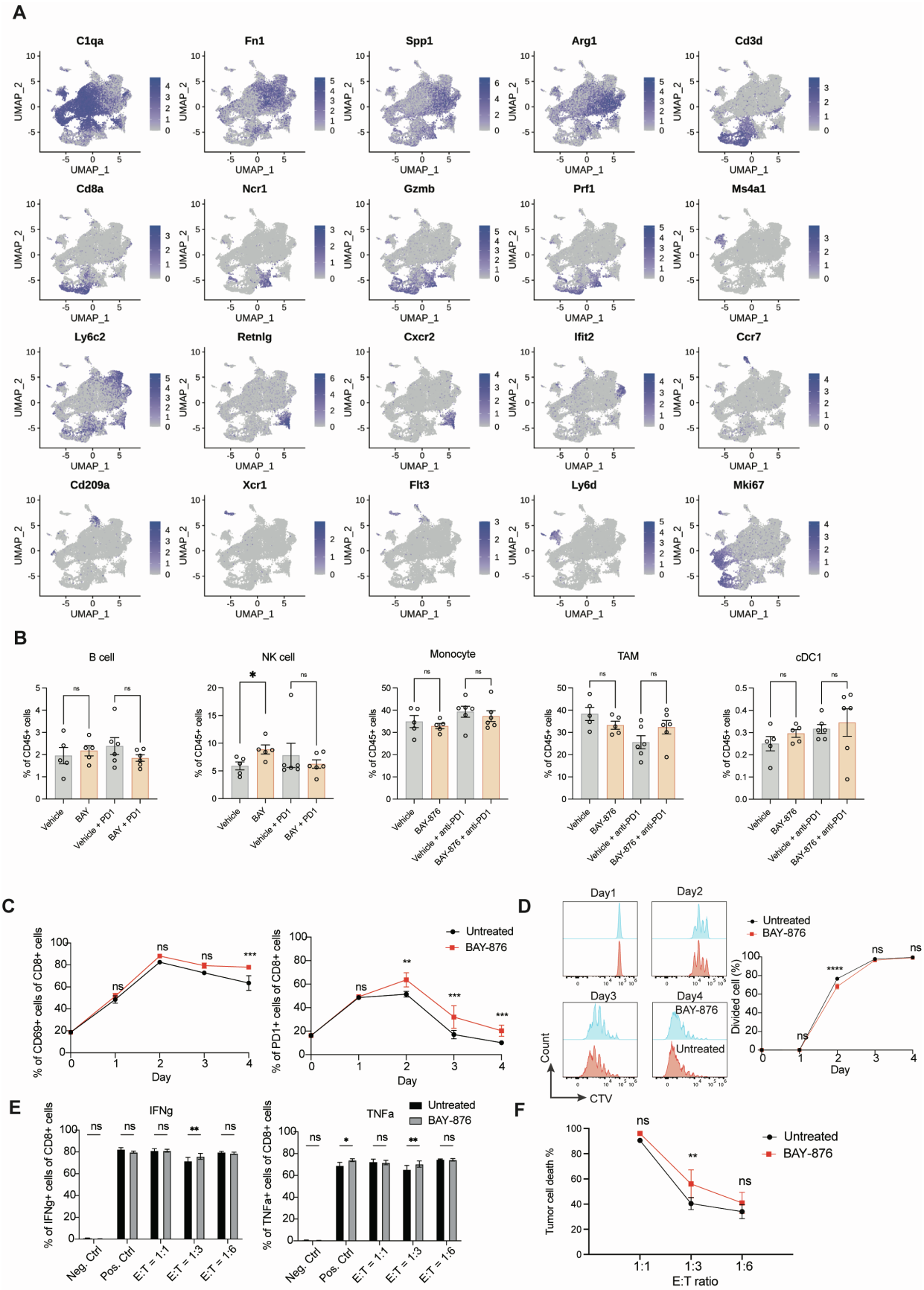
A
C1qa
Fn1
Spp1
Arg1
Cd3d
Cd8a
Ncr1
Gzmb
Prf1
Ms4a1
Ly6c2
Retnlg
Cxcr2
Ifit2
Ccr7
Cd209a
Xcr1
Flt3
Ly6d
Mki67
UMAP_1
UMAP_2
B
B cell
NK cell
Monocyte
TAM
cDC1
% of CD45+ cells
Vehicle
BAY
Vehicle + PD1
BAY + PD1
BAY-876
Vehicle + anti-PD1
BAY-876 + anti-PD1
C
% of CD69+ cells of CD8+ cells
% of PD1+ cells of CD8+ cells
Day
Untreated
BAY-876
D
Day1
Day2
Day3
Day4
Count
CTV
Divided cell (%)
E
IFNg
TNFa
% of IFNg+ cells of CD8+ cells
% of TNFa+ cells of CD8+ cells
Neg. Ctrl
Pos. Ctrl
E:T = 1:1
E:T = 1:3
E:T = 1:6
F
Tumor cell death %
E:T ratio

Figure S6. The impact of Glut1 inhibition on the tumor microenvironment, Related to Figure 6.

(**A**) UMAP plots showing expression of key markers in clusters from Figure 6E.

(**B**) Summary of flow cytometry analysis of the relative percentage of infiltrated immune cells in CD45+ compartment (n = 5-6).

(**C-D**) Naïve OT-I CD8+ T cells were activated in the presence or absence of 200nM BAY-876 for 4 days. The percentage of CD69+ and PD-1+ cells were determined by FACS (C, n = 3). The proliferation of T cells was determined by CTV dilution experiment (D, n = 3).

(**E-F**) Activated T cells were pretreated with 200nM BAY-876 for 24 hours, and then co-cultured with SIINFEKL pulsed LLC tumor cells with the indicated E:T ratio and PMA stimulation as positive control in the presence of BAY-876. The percentage of IFNγ+ and TNFα+ T cells (E, n = 4) and tumor killing (F, n = 4) were quantified by FACS.

Data are represented as means $\pm$ SEM in (B) and means $\pm$ SD in (C-F). *P < 0.05, **P < 0.01, ***P < 0.001 and ****P < 0.0001 by unpaired Student's t test in (B), and by two-way ANOVA in (C-F). n.s., not significant.

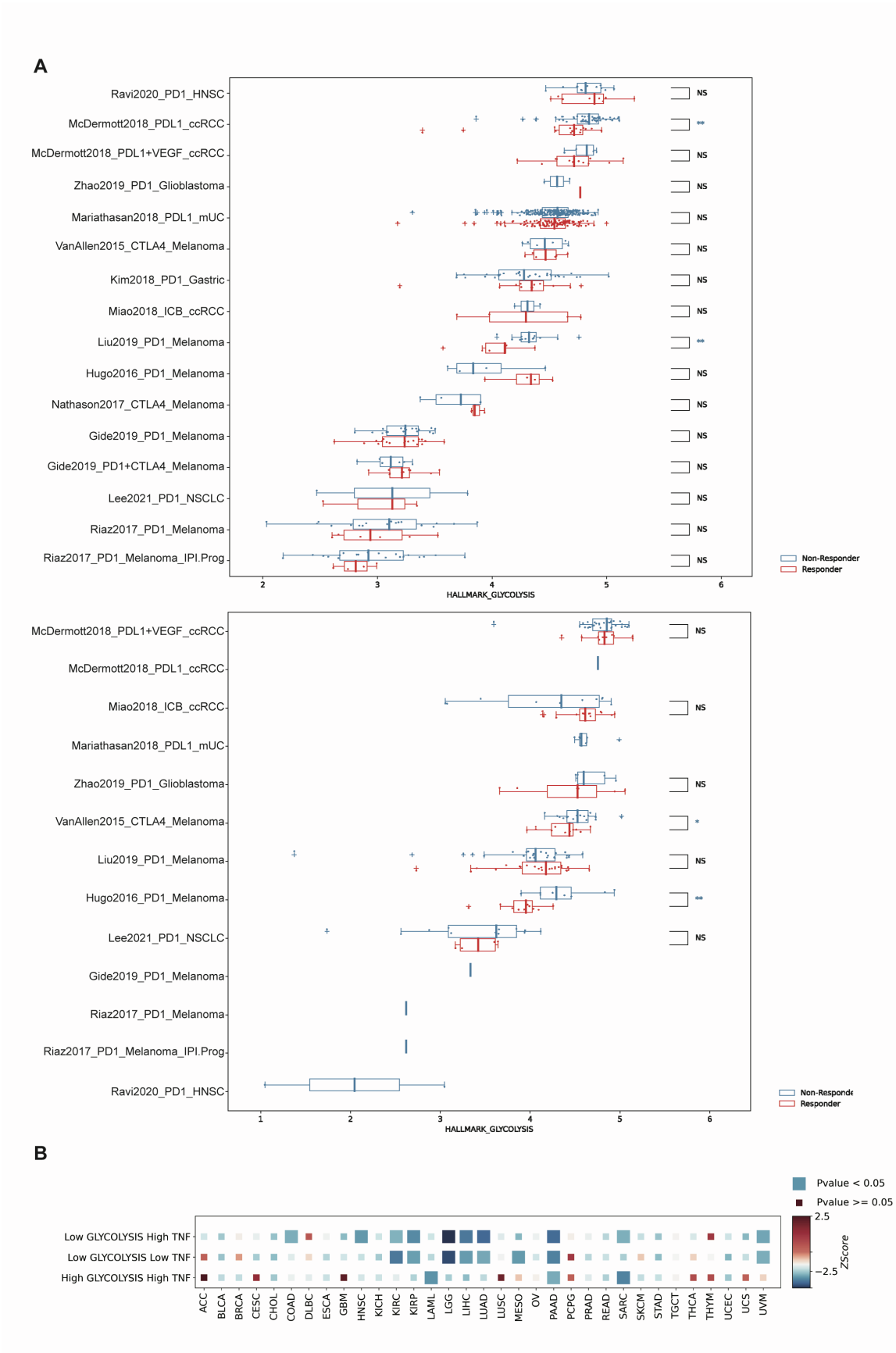
A
Ravi2020_PD1_HNSC
McDermott2018_PDL1_ccRCC
McDermott2018_PDL1+VEGF_ccRCC
Zhao2019_PD1_Glioblastoma
Mariathasan2018_PDL1_mUC
VanAllen2015_CTLA4_Melanoma
Kim2018_PD1_Gastric
Miao2018_ICB_ccRCC
Liu2019_PD1_Melanoma
Hugo2016_PD1_Melanoma
Nathason2017_CTLA4_Melanoma
Gide2019_PD1_Melanoma
Gide2019_PD1+CTLA4_Melanoma
Lee2021_PD1_NSCLC
Riaz2017_PD1_Melanoma
Riaz2017_PD1_Melanoma_IPI.Prog
NS
**
2
3
4
5
6
HALLMARK_GLYCOLYSIS
Non-Responder
Responder
McDermott2018_PDL1+VEGF_ccRCC
McDermott2018_PDL1_ccRCC
Miao2018_ICB_ccRCC
Mariathasan2018_PDL1_mUC
Zhao2019_PD1_Glioblastoma
VanAllen2015_CTLA4_Melanoma
Liu2019_PD1_Melanoma
Hugo2016_PD1_Melanoma
Lee2021_PD1_NSCLC
Gide2019_PD1_Melanoma
Riaz2017_PD1_Melanoma
Riaz2017_PD1_Melanoma_IPI.Prog
Ravi2020_PD1_HNSC
NS
*
**
1
2
3
4
5
6
HALLMARK_GLYCOLYSIS
Non-Responde
Responder
B
Pvalue < 0.05
Pvalue >= 0.05
2.5
−2.5
ZScore
Low GLYCOLYSIS High TNF
Low GLYCOLYSIS Low TNF
High GLYCOLYSIS High TNF
ACC
BLCA
BRCA
CESC
CHOL
COAD
DLBC
ESCA
GBM
HNSC
KICH
KIRC
KIRP
LAML
LGG
LIHC
LUAD
LUSC
MESO
OV
PAAD
PCPG
PRAD
READ
SARC
SKCM
STAD
TGCT
THCA
THYM
UCEC
UCS
UVM

Figure S7. The relevance of TNFα and glycolysis interaction in human, Related to Figure 7.

(**A**) HALLMARK_GLYCOLYSIS expression level of the responders and non-responders of immune-cold (up) and -hot (down) cohorts, which were defined by CTL level that was calculated by the average expression of CD8A, CD8B, GZMA, GZMB, and PRF1. (**B**) Heatmap showing the association of survival time of TCGA cohorts and the level of HALLMARK_GLYCOLYSIS and TNFα. Z scores and p values are derived from Cox proportional-hazards model which takes the $Glycolysis^{high}$/ TNF^{low} group as the reference level. Negative z scores indicate longer survival time compared to the $Glycolysis^{high}$/ TNF^{low} group.

Data are represented as means ± SD. *P < 0.05, **P < 0.01, ***P < 0.001 and ****P < 0.0001 by linear regression model which uses HALLMARK_GLYCOLYSIS expression level to predict responding status (responder vs. non-responder). n.s., not significant.

Table S1. Summary of human sample information, related to STAR method.

Sample ID	*Gender*	*Age*	*Diagnosis*	*Pathologic Staging (pTNM)*
21-46279	Female	53	Lung adenocarcinoma	pT2bN0Mx
21-45919	Male	69	Lung adenocarcinoma	pT1cN0Mx
21-43598	Male	70	Lung adenocarcinoma	pT1bN0Mx
21-41981	Female	68	Lung adenocarcinoma	pT1bN0Mx
21-42927	Male	73	Lung adenocarcinoma	pT4N2Mx
21-39799	Male	67	Lung adenocarcinoma	pT1bN0Mx
21-45808	Male	66	Lung adenocarcinoma	pT1cN0Mx
21-45788	Male	60	Lung adenocarcinoma	pT3N0Mx
21-38356	Male	69	Lung adenocarcinoma	pT2bN0Mx
21-34724	Male	73	Lung adenosquamous carcinoma	pT2N0Mx
21-28132	Male	41	Pancreatic ductal adenocarcinoma	T4N1M0
21-38600	Male	58	Pancreatic ductal adenocarcinoma	pT2N2Mx
21-17181	Male	59	Pancreatic ductal adenocarcinoma	pT2N2Mx
21-19748	Female	62	Pancreatic ductal adenocarcinoma	pT2N1Mx
21-17601	Male	58	Pancreatic ductal adenocarcinoma	pT2N0Mx
21-41396	Male	61	Pancreatic ductal adenocarcinoma	pT4N2Mx
21-05979	Female	63	Pancreatic ductal adenocarcinoma	pT2N0Mx
21-38360	Male	70	Pancreatic ductal adenocarcinoma	pT3N1Mx
21-13930	Male	74	Pancreatic ductal adenocarcinoma	pT2N0Mx
21-44605	Female	58	Pancreatic ductal adenocarcinoma	pT1cN1Mx
22-07399	Male	69	Colon adenocarcinoma	pT3N0Mx
22-00849	Male	56	Colon adenocarcinoma	pT3N0Mx
22-05396	Female	64	Colon adenocarcinoma	pT3N0Mx
21-46248	Male	69	Colon adenocarcinoma	pT3N1cMx
21-46144	Female	70	Colon adenocarcinoma	pT2aN0Mx
21-46241	Female	65	Colon adenocarcinoma	pT4aN2bMx
22-03448	Female	71	Colon adenocarcinoma	Rectal tumor pT1N0Mx; Right hemicolectomy tumor; pT3N0Mx
21-43098	Male	63	Colon adenocarcinoma	pT3N0Mx

21-42151	Male	72	Colon adenocarcinoma	pT3N2Mx
21-42916	Female	56	Colon adenocarcinoma	pT3N0Mx

Table S2. Summary of sgRNA sequence used in this study, related to STAR method.

sgRNA name	*Sequence (5'-3')*
sgGlut1-1	TCAGCATGGAGTTCCGCCTG
sgGlut1-2	GTGTCACCTACAGCTCTACG
sgGpi1-1	ACTTACCGTGTTCGTAGACA
sgGpi1-2	GTACACTGGCAAATCCATCA
sgTnfrsr1a	GGATCCCGTGCCTGTCAAAG
sgCasp8	TGAGATCCCCAAATGTAAGC
sgFadd	TAGATCGTGTCGGCGCAGCG
sgRipk1	GGGTCTTTAGCACGTGCATC
sgRipk3	GTGGGACTTCGTGTCCGGGC
sgControl-1	TTTTCGTCGACTAAGTCAAG
sgControl-2	AAGATCCTCTCGGCGTTTAT
sgGlut3	TGCCCTCTGGTCCTTATGTG

Table S3. Human scRNA-seq datasets, related to STAR method.

Deposited data	**Source**	**Identifier**
Human NSCLC scRNA-seq dataset	Lambrechts et al., 2018 [58] PMID: 29988129	ArrayExpress: E-MTAB-6149
	Song et al., 2019 [59] PMID: 31033233	GEO: GSE117570
	Zilionis et al., 2019 [60] PMID: 30979687	GEO: GSE127465
	Wang et al., 2020	GEO: GSE143423

	Chi et al., 2020 [61] PMID: 32675368	GEO: GSE150660
Human PAAD scRNA-seq dataset	Peng et al., 2019 [62] PMID: 31273297	GSA: CRA001160
	Moncada et al., 2020 [63] PMID: 31932730	GEO: GSE111672
	Schlesinger et al., 2020 [64] PMID: 32908137	GEO: GSE141017
	Lin et al., 2020 [65] PMID: 32988401	GEO: GSE154778
Human breast cancer scRNA-seq dataset	Chung et al., 2017 [66] PMID: 28474673	GEO: GSE75688

Table S4. Human ICB datasets, related to STAR method.

Source	**ICB cohorts**
PMID: 29443960 [55]	Mariathasan2018_PDL1_mUC
PMID: 29301960 [67]	Miao2018_ICB_ccRCC
PMID: 26359337 [68]	VanAllen2015_CTLA4_Melanoma
PMID: 30753825 [69]	Gide2019_PD1_Melanoma
	Gide2019_PD1+CTLA4_Melanoma
PMID: 29867230 [70]	McDermott2018_PDL1_ccRCC
	McDermott2018_PDL1+VEGF_ccRCC
PMID: 30742119 [71]	Zhao2019_PD1_Glioblastoma

PMID: 31792460 [72]	Liu2019_PD1_Melanoma
PMID: 26997480 [73]	Hugo2016_PD1_Melanoma
PMID: 29033130 [74]	Riaz2017_PD1_Melanoma
	Riaz2017_PD1_Melanoma_Ipi.Prog
PMID: 30013197 [75]	Kim2018_PD1_Gastric
PMID: 27956380 [76]	Nathanson2017_CTLA4_Melanoma
PMID: 32665297 [77]	Ravi2020_PD1_HNSC
PMID: 33857424 [78]	Lee2021_PD1_NSCLC